PREDICTION OF SOUND PRESSURE AND INTENSITY FIELDS IN ROOMS AND NEAR SURFACES BY RAY TRACING

by

Owen Mathew Cousins

B.Sc., The University of British Columbia, 2005

A THESIS SUBMITTED IN PARTIAL FULFILMENT OF
THE REQUIREMENTS FOR THE DEGREE OF

Master of Applied Science

in

The Faculty of Graduate Studies

(Mechanical Engineering)

The University of British Columbia

(Vancouver)

April 2008

Abstract

The health, safety, comfort and productivity of a room's occupants is greatly influenced by the sound field within it. An acoustical engineer is often consulted during the design of a room to prevent or alleviate unwanted acoustical problems. Prediction models are often used to find the most cost-effective solution to a given acoustical problem. The accuracy of sound-field prediction varies with the particular model, as do the parameters predicted. Most models only predict sound-pressure levels. Many only predict energetic quantities, ignoring wave phase and, therefore, interference and modal effects in rooms. A ray-tracing model, capable of predicting sound-pressure level, reverberation time and lateral energy fraction was translated into MATLAB code and modified to increase accuracy by including phase. Modifications included phase effects due to path length travelled and phase changes imparted by surface reflections as described by complex reflection coefficients. Further modifications included predicting steady-state and transient sound-intensity levels, providing information on the direction of sound-energy flow. The modifications were validated in comparison with free-field theory and theoretical predictions of sound fields in the presence of a single surface. The complex reflection coefficients of four common building materials were measured using two methods—an impedance tube and the spherical-decoupling method. Using these coefficients, the modified program was compared with experimental data measured in configurations involving one or more surfaces made of these materials, in an anechoic chamber, a scale-model room, and a full-scale office space. Prediction accuracy in the anechoic chamber, and in the presence of a single reflecting surface, greatly improved with the inclusion of phase. Further comparison with full-scale rooms is required before the accuracy of the model in such rooms can be evaluated definitively.

Table of Contents

List of Tables

List of Figures

List of Symbols

c	speed of sound
λ	wavelength
f	frequency
s	condensation
$\vec{u}$	particle velocity
ρ_o	equilibrium density
P	instantaneous density
ν	ratio of specific heats
B	bulk modulus
t	time
ω	angular frequency
k	wave number
F	force
Z	characteristic impedance
P	sound pressure
$\vec{I}$	acoustic intensity
Z_s	normal surface impedance
R	reflection coefficient
α	absorption coefficient
SPL	sound pressure level
L_p	sound pressure level
SIL	sound intensity level
L_I	sound intensity level
E_{ray}	energy of a ray
L_W	sound power level
W	sound power
N	total number of rays
n	number of received rays
V	volume of the receiver cell
D	total source to receiver distance traveled
H	air absorption coefficient
L	receiver cell side length

Acknowledgments

This research has had its ups and downs, at times it seemed there was no foreseeable end to the program bugs, experimental work, or format issues of this thesis. There are many people without whom I could not have completed my objectives, and for that I am very gratefull.

To my graduate supervisor at UBC, Dr. Murray Hodgson, thank you very much. This project, this degree, would not have begun in the first place without your support and interest. Your continuing efforts to assist me in any regard, and expertise is very much appreciated. My knowledge of acoustics has arisen in its entirety thanks to you.

To Gary Chan, Gavin Steininger, and Alireza Khalegi, and everyone else in the acoustics lab, thank you very much for your insight, your knowledge on what must have seemed like trivial questions, and the opportunities for quick social reprieves from the occasionally mundane work.

To my parents, your enthusiasm and support throughout the years brought me to university in the first place. That support has remained constant throughout this entire process, I would not have finished any schooling if it were not for the values you taught me while growing up, not to mention the warm meals offered on weekends.

To Krystle Taylor, you only had to witness first hand the final year of this work, but I do not consider it a coincidence that it was the year that you spent with me that resulted in the greatest progress. Thank you for your enthusiasm, high spirits, and pressure to finish. You made an excellent volunteer lab partner, I can only hope my career is spent with coworkers who are as committed and diligent as you. Your continued encouragement throughout the future years will enable me to accomplish very much.

Owen Cousins
April, 2008.

Chapter 1

Introduction

1.1 Background and motivation

Historically, the sound-absorption characteristics of many materials have been investigated extensively, with the majority of research being the calculation of the dissipation of sound energy from a system. There exist multiple standards for the measurement of absorption coefficients, aimed at standardizing the measurement of the exact proportion of energy absorbed when a sound wave is incident on a surface, for example, in a room. Since the investigation of interference effects and modal behaviour in a room depends on the phase, not only the magnitude, of propagating sound waves, knowledge of the complex reflection coefficients (RCs) of surfaces is vital. Sound fields within enclosed spaces are better modeled using the complex reflection coefficient, and not just the absorption coefficient.

Various reflection properties of room surfaces are of critical importance when considering acoustics in room design. Reflection coefficients, along with room size and shape, are key properties which influence an acoustically conscious architect when designing spaces such as concert halls, studios, classrooms and offices. When optimizing a soundscape, important surface characteristics are not only the absorption and reflection coefficients, but also include the diffusion coefficient, a measure of the extent to which a surface reflects sound diffusely. For example, diffusing reflectors on certain surfaces of a concert hall can be used to break up standing-wave effects, reduce reverberation, and increase the spatial impression of the listener.

A good design of any acoustical environment usually begins with good prediction work to optimize room dimensions, surface treatments, and/or source and occupant locations. With growing computational power, sound-field predictions are becoming increasingly accurate, but many still suffer from being based on inaccurate or oversimplified physical models, and the requirement of user-input parameters to describe surfaces. Input parameters are often poorly estimated by the user. Prediction models

vary as greatly in their implementation as they do in their accuracy. They ideally account for the spherical spreading of sound, air absorption, phase due to path-length traveled and phase shift upon reflection, the absorption and diffusion characteristics of the room surfaces, and the dependence of the surface properties on angle of sound incidence. Prediction model accuracy is limited by the accuracy of the user-input parameters. Using experimentally measured reflection coefficients of the surfaces in a room provides the most accurate results.

The room occupant's acoustical experience does not solely depend on sound-pressure levels, but is also affected by the direction in which sound energy is propagating at their location. The sound-intensity level is a measure which provides information on the amplitude and the direction of energy flow. It allows one to predict the perceived sound source location.

The research presented in this work is greatly motivated by a need to predict room sound fields more accurately. A ray-tracing prediction model was translated, modified, validated, and compared with measured sound fields in an effort to do so.

1.2 Aim and methodology

In the first part of this thesis, the physics of sound in rooms will be introduced. The acoustical wave equation will be derived, and the way sound propagates and meets surfaces will be described. Various prediction models will be discussed briefly, including their drawbacks and inaccuracies. Numerous improvements will be proposed for a ray-tracing program and their implementation discussed.

The second part covers, in detail, the analysis of the new prediction model. This begins by validating the implementation of the physics modeled and assessing its accuracy, before comparing sound-pressure and intensity levels predicted with those measured in an anechoic chamber and in test rooms.

Finally, conclusions are drawn on the accuracy of the modified program, and suggestions for its future use are given.

Chapter 2

Definitions and physical concepts

Prior to the discussion of prediction models and their strengths and weaknesses, the laws of acoustical wave propagation in rooms need to be discussed. This will be the topic of this chapter.

2.1 Defining sound

An acoustic wave is a pressure disturbance propagating throughout an elastic medium. Although sound waves can propagate through solids, this work is concerned with the sound fields within rooms and therefore is interested solely on the propagation of sound in fluids such as air. In fluids, sounds are longitudinal waves, and cause the molecules of a medium to move back and forth in the direction of propagation, creating zones of compression and rarefaction.

A *particle of fluid* is a finite volume of fluid that is both small enough that acoustical variables can be considered constant within it, but large enough to consider the particle homogenous and isotropic. A small volume of homogenous, isotropic, elastic, and compressible air has some important characteristics. This volume has mass, does not support shear force, is perfectly elastic; if compressed it distributes that pressure uniformly, and the applied pressure is proportional to the change in its volume. When a vibrating object is placed in a fluid, it accelerates neighbouring particles which, in turn, accelerate their neighbours. Momentum is transferred, the outcome of which is a wave of compression and rarefaction that propagates away from the vibrating object. This wave propagates at the speed of sound (c). Two points in this wave are considered in phase when they are separated by an integral number of wavelengths (λ) defined as:

$$\lambda = c / f \tag{2.1}$$

where f is the frequency of vibration in cycles per second (Hz). *Sound pressure* is the difference in pressure between the ambient or static pressure of the volume and the

instantaneous pressure while an acoustical wave propagates through it. *Particle velocity* is not the velocity of the individual air molecules, but is instead the velocity of the entire particle of fluid as it is displaced by sound.

2.2 The wave equation

Three equations are required to derive the acoustical wave equation, solutions to which describe the propagation of sound. They are:

Continuity Equation $$\frac{\partial s}{\partial t} + \nabla \bullet \vec{u} = 0 \tag{2.2}$$

Euler's Equation $$\rho_o \frac{\partial \vec{u}}{\partial t} = -\nabla P \tag{2.3}$$

Equation of State $$P = P_o \gamma s = B s \tag{2.4}$$

where $s = (\rho - \rho_0)/\rho_0$ is the condensation, $\vec{u}$ is the particle velocity, ρ_0 is the equilibrium density, P is the instantaneous pressure, P_o is the equilibrium pressure, γ is the ratio of specific heats, and $B = P_o \gamma$ is the bulk modulus of the fluid. The wave equation can be first derived in 1D and then expanded to 3D. Assuming the wave is traveling in the x direction, Eq. (2.4) can be differentiated with respect to time, and s can be eliminated by substituting Eq. (2.2) to give:

$$\frac{\partial P}{\partial t} = -\gamma P_o \nabla \bullet \vec{u} \tag{2.5}$$

If Eq. (2.5) is differentiated with respect to time, and the 1D equivalent of Eq. (2.3) is differentiated with respect to x, u can be eliminated to produce:

$$\frac{\partial^2 P}{\partial t^2} = \frac{\gamma P_o}{\rho_o} \frac{\partial^2 P}{\partial x^2} \tag{2.6}$$

Since the speed of sound $c = \sqrt{\frac{\gamma P_o}{\rho_o}}$ we can substitute to find the 1D wave equation:

$$\frac{\partial^2 P}{\partial t^2} = c^2 \frac{\partial^2 P}{\partial x^2} \tag{2.7}$$

which, when expanded to 3D, equals:

$$\frac{\partial^2 P}{\partial t^2} = c^2 \nabla^2 P \tag{2.8}$$

2.3 Harmonic solution to the wave equation

If the wave variables such as pressure vary sinusoidally, the wave is harmonic and therefore has a harmonic solution dependent on ω , the angular frequency. For plane waves, the solution can be written as:

$$P(x,t) = Ae^{i(\omega t - kx)} + Be^{i(\omega t + kx)} \tag{2.9}$$

where $k = \omega / c$ is called the *wave number*. This solution can be expanded for wave propagation in any direction by defining $|k| = \sqrt{k_x^2 + k_y^2 + k_z^2} = \omega / c$ so that:

$$P(r,t) = Ae^{i(\omega t - k \bullet \bar{r})} \tag{2.10}$$

The solution above does not contain any source term, which is necessary for any acoustical disturbance to exist. If the source is inside the room, compression and rarefaction waves can be created by two mechanisms. The empty volume of the room can change sinusoidally with time - such is the case when a completely enclosed loudspeaker is placed in a room - or a force can be applied directly to the fluid - such is the case with the vibrating cone of an unbaffled loudspeaker. An unbaffled cone moving back and forth does not change the empty volume of the room since any void created as it

drives backwards is replaced by the removed volume behind the cone. The source terms can simply be added to the right hand side of the homogeneous solution, such as:

$$\nabla^2 P - \frac{1}{c^2}\frac{\partial^2 P}{\partial t^2} = -\frac{\partial G}{\partial t} + \nabla \cdot F \tag{2.11}$$

where $-\frac{\partial G}{\partial t}$ represents the change in volume with respect to time and $\nabla \cdot F$ represents the force term.

2.4 Acoustical quantities

The ratio of the complex pressure to the particle velocity is called the S*pecific impedance*. If a plane wave is traveling through a homogenous fluid then this ratio is called the *Characteristic impedance* since it is a characteristic property of the fluid, denoted by *Z*. In air, *Z* is a real number that is independent of frequency, provided that air is considered a lossless fluid. Since Z_{air} is real, pressure and particle velocity are in phase:

$$Z = P/u = \rho c \tag{2.12}$$

The *Acoustic intensity* is a vector quantity that equals the average rate of energy flow across a surface of unit area in that direction. It is found by multiplying the time averaged acoustical pressure by the particle velocity:

$$I = \overline{Pu} \tag{2.13}$$

When a sound wave in air is incident on a plane boundary, the direction and strength with which it reflects is dependent upon the surface impedance of the boundary. Defined as the complex ratio of pressure amplitude at the boundary to the particle velocity normal to the surface, the *(normal) surface impedance*, Z_s, can be described as either *locally reacting* or *extended reacting*. The former is the case if the (normal) surface impedance is independent of angle of incidence, while in the latter case it is

dependent. Provided the surface impedance is known for all angles of incidence, the sound field in the volume in front of the boundary can be calculated.

R, defined as the complex ratio of the amplitudes of the incoming and outgoing pressure waves, is called the *reflection coefficient* of the surface. Using laws of continuity of pressure and particle velocity at the boundary of the surface, *R* can be calculated using the surface impedance as follows (De Geetere [1]):

$$R = \frac{(Z_s \cos(\theta) - Z_{air})}{(Z_s \cos(\theta) + Z_{air})} \tag{2.14}$$

Since Z_s is often a complex value, so too is *R*, which can have a real part ranging from -1 to +1. For rigid surfaces, Z_s becomes very large and *R* approaches +1 regardless of angle of incidence, representing total reflection without attenuation of the pressure amplitude. Soft boundaries such as the seabed are dubbed *pressure release boundaries,* since their reflection coefficient approaches -1. An *R* value of -1 still represents complete reflection, but the pressure wave suffers a 180° phase change since, at boundaries of pressure release, there does not exist a boundary condition of zero particle velocity. This in turn means the condition of maximum pressure does not apply. Any *R* value with a real part between -1 and +1 represents a reflection, either with or without the 180° phase change, where the reflected pressure wave is also attenuated. Further phase delay is imparted on a reflected sound wave if *R* is complex, since a complex reflection coefficient will change the imaginary part, and therefore the phase, of a propagating sound wave.

The *absorption coefficient*, α, of a surface is defined as the percentage of sound energy that is absorbed by the surface when a sound wave strikes it. α is calculated from *R*, which in turn was defined by Z_s. For plane waves, α is found to be (De Geetere [1]):

$$a(\theta) = 1 - |R(\theta, Z_s)|^2 \tag{2.15}$$

Sound-pressure level (SPL) is a logarithmic measure of pressure normalized such that 0 dB is the r.m.s. pressure of a 1000 Hz sound wave that is just audible ($P_o = 2 \times 10^{-5}$ Pa):

$$L_p = 10\log\left(\frac{P^2}{P_o^2}\right) \tag{2.16}$$

The *sound-intensity level* (SIL) is normalized similarly (I_o = 10^{-12} Watts/m^2):

$$L_I = 10\log\left(\frac{W}{I_o}\right) \tag{2.17}$$

SIL is equal to the SPL in free-field or anechoic environments when plane sound waves propagate away from the source. The sound power level, L_w , is similarly defined (W_o = 10^{-12} Watts):

$$L_W = 10\log\left(\frac{W}{W_o}\right) \tag{2.18}$$

2.5 Sound sources and waves

Two common wave forms that are observed are plane waves and spherical waves. Plane waves arise from the vibration of an infinite plane where all the parts of the plane move in unison. The solutions to the wave equation in Cartesian coordinates:

$$\frac{(\partial^2 P)}{(\partial x^2)} + \frac{(\partial^2 P)}{(\partial y^2)} + \frac{(\partial^2 P)}{(\partial z^2)} - \frac{1}{(c^2)}\frac{(\partial^2 P)}{(\partial t^2)} = 0 \tag{2.19}$$

are found to be (for propagation in the x direction):

$$P(x,t) = Ae^{i(wt-kx)} + Be^{i(wt+kx)} \tag{2.20}$$

$$\vec{U}(x,t) = P\frac{(x,t)}{(\rho_o c)} \tag{2.21}$$

Some important conclusions can be drawn; they are:

- The amplitudes of pressure and velocity do not depend on distance;
- Pressure and velocity are in phase;
- The specific impedance $P/U = \rho_o c$.

Chapter 2

Spherical waves are created by a point source or by any spherical vibrating surface on which all parts move in phase. The radial wave equation in spherical coordinates reduces to:

$$\frac{\partial^2(rP)}{\partial r^2}-\frac{1}{c^2}\frac{\partial^2(rP)}{\partial t^2}=0 \tag{2.22}$$

which has the solutions:

$$P(r,t)=\frac{P}{r}e^{i(wt-kr)} \tag{2.23}$$

$$\vec{U}(r,t)=(1-\frac{i\lambda}{2\pi r})(\frac{P(r,t)}{\rho_o c}) \tag{2.24}$$

Characteristics of these solutions to note are:

- Pressure and velocity amplitudes are inversely proportional to *r*;
- The sound-pressure level drops 6 dB for every doubling of distance;
- The first term approaches 1 for values of r that are much greater than $\lambda/2\pi$; after this point (the far field), pressure and velocity are in phase, as they were for a planar sound wave, otherwise they are not in phase (near-field).

Chapter 3

Background and objectives

3.1 Literature review

A detailed review of the literature on the development of various room prediction models was conducted to gain an understanding of the options an acoustician has when it is necessary to predict a room sound field. This review highlighted the general cases when certain models performed particularly well, and when they did not. Articles of interest were focused on early developments of each model type, as well as any modifications that were made to improve their accuracy.

Room prediction models can be grouped into one of two general approaches, or perhaps a combination of the two. The first approach to solving for a sound field is wave-based. That is to say that the pressure is found with respect to time and position by directly solving the wave equation with appropriate boundary conditions. These solutions are well known and exact; an example of finding such solutions is given by Kuttruff [2] for rectangular rooms. This approach is only suitable for rectangular rooms at relatively low frequency, due to the extensive complexity of finding these solutions.

Another way to solve the wave equation is to do it numerically using either a Finite Element Method (FEM) or a Boundary Element Method (BEM). This method is applicable to rooms of any geometry, but is still limited to low frequency in order to have enough elements per wavelength and small room volumes to prevent excessive run times (Hamdi and Mebarek [3])**.**

The second approach to solving a room sound field is geometric-based. According to this strategy it is necessary to replace waves with the concept of sound rays; these are tracked as they reflect around the room, their energies being summed as each ray is received. Since these approaches are traditionally energy-based, phase effects are ignored; therefore this approach is only valid at high frequencies for which the sound field is more diffuse, having indistinguishable nodal patterns.

One example of a geometric approach is the Method of Images (MOI) presented by Allen and Berkely [4]. This method replaces boundary surfaces with mirror-image sources, and adds the direct contributions of each and every image source. This method presents the exact solution for rectangular, highly reflective surfaces where sound-wave reflection occurs specularly.

Ray tracing models, such as the one created by Ondet and Barbry [5]**,** are another geometric approach to solving a room's sound field. This method traces source – receiver paths by tracking omni-directionally emitted rays from a source to a receiver, adding their contributions. This method is valid for rooms of any geometry but, since rays are dimensionless a receiver with a non-zero volume must be used introducing errors due to temporal and spatial averaging. As is the case for all energy-based models, ray tracing is limited to higher frequencies.

Beam tracing, as described by Farina [6], is similar to ray tracing, but beams with finite cross-sectional areas are used, as opposed to dimensional rays. A source is divided into a triangular-faced surface, each facet representing the base of one beam. This method permits the use of point receivers and prevents a ray-divergence problem. Unfortunately, this approach suffers from difficulties when a beam strikes more than one plane (eg. a corner), therefore presenting two or more directions in which to reflect. Most algorithms assume that a beam follows the path of a ray at its centre; nevertheless, this can lead to either too little or too much energy being received.

All previous geometric models are limited to higher frequencies, since phase effects are ignored. Since their early development, many models have been modified to lower the frequency limits by accounting for phase effects.

An image-phase model, developed by Suh and Nelson [7], was shown to dramatically increase the lower frequency accuracy of image models by giving each image source a representative phase. This model is still limited to purely specular reflection.

A beam-tracing model, developed by Wareing [8], was created to predict sound-pressure levels including phase and interference effects and surfaces of extended reaction as described by angularly-varying complex pressure-reflection coefficients. Accuracy at

lower frequency greatly increased, but the model is only capable of predicting the sound-pressure level at a single location. This model also assumes specular reflecting surfaces; therefore rooms with diffusely reflecting surfaces are not modeled.

A Modal model was developed by Wong [9] to predict sound-pressure levels in a room including a point source. This model included phase and lightly-damped surfaces. The Helmholtz equation for the eigen-functions of a rigid-walled enclosure is solved using a Green's Function to find an expression for the pressure at any point within a room. This model works for empty rooms only; the effect of room fittings is not modeled.

In other work, the original ray-tracing program developed by the Ondet and Barbry [5] has been modified by Hodgson [10] to include diffuse reflection which he termed DRAYCUB, the calculation of the sound echogram (variation of squared-pressure with time of arrival) and, from it, sound-decay curves, reverberation time, lateral energy fractions, and other acoustical quantities, this version called ERAYCUB. Despite these various improvements, this program still ignores phase and is therefore applicable to higher frequency ranges only. The same program was later modified to include the calculation of speech intelligibility. Chan [11] later translated the DRAYCUB into a MATLAB file, and then implemented a diffraction model within it.

3.2 Research Objectives

The review of the aforementioned literature provided evidence that prediction models are still insufficiently accurate. A room prediction model that accounts for phase effects, complex reflection coefficients, diffuse reflections, room fittings, which predicts sound intensities, as well as sound-pressure levels, for rooms of any shape and size, does not exist.

The detailed objectives of this research were reached upon review of the literature on room prediction models. These objectives included:

- Translating the ERAYCUB program to MATLAB

- Modifying a ray-tracing program to account for the phase of propagating rays (and therefore, interference effects due to path-length differences between received rays);
- Modifying a ray-tracing program to include phase change of a ray on reflection from a surface of non-infinite impedance;
- Modifying a ray-tracing program to include the prediction of both steady-state and transient intensity levels;
- Validating the updated model by comparing prediction with theory;
- Comparing predicted sound-pressure levels and sound-intensity levels to those measured for numerous test cases;
- Analyze and draw conclusions on the accuracy and effectiveness of the modified ray tracing-program.

The starting point of the work was Chan's MATLAB version of the Ondet and Barbry model. The following chapters include the development and implementation of the above objectives in chapter 4, the results of validation and comparison attempts in chapters 5 and 6, a discussion of error sources in chapter 7; conclusions are drawn in chapter 8 and finally, future work is suggested.

Chapter 4

Ray-tracing model development

Starting with Chan's MATLAB implementation of the Ondet and Barbry algorithm, the model was modified to account for phase effects and to predict intensity. The original model and the improvements made are discussed in this chapter.

4.1 Existing ray-tracing prediction model

The improved prediction model was based on RAYCUB, an energy-based ray-tracing prediction model. Created by the National Institute for Research on Safety (INRS) France in the early eighties, RAYCUB predicts SPLs at one, or any number of cubic receiver volumes on a horizontal plane within a room. The user must define the boundary conditions, which include surface locations, energy reflection coefficients for each surface, and the location of any partitions that may be present. Other input parameters include air-absorption coefficients, sound-source locations, receiver-cell size, the number of rays to be emitted (omni-directionally) from each source, and the number of reflections to be tracked for each ray. The accuracy of the model is greatly increased by increasing both the number of rays, and the number of trajectories followed. SPLs at user-defined locations are calculated for up to eight cases (eg. frequencies or different reflection coefficients).

RAYCUB is implemented such that the given number of rays is emitted from the source in random directions. Each ray is tracked by calculating the first surface it strikes, checking if a receiver volume is crossed, and then reflecting that ray at a specular angle after attenuating its energy by multiplying it by the user-defined reflection coefficient for that surface. This process is repeated for the given number of reflections. If a receiver volume is crossed in any one trajectory, the energy of the ray at that point, attenuated by spherical spreading, air absorption and previous surface reflections, is added to the total SPL for that receiver.

Chapter 4

RAYCUB has since been modified (Hodgson [10]) to include, among other things, the calculation of echogram, sound decay-curves, reverberation time, speech-intelligibility index, and early-decay time. The program was also modified to include diffuse reflection, an important change due to the fact that surfaces may not reflect specularly. Some surfaces, such as rough or porous media, reflect incoming sound waves at angles other than specular (Cremer and Muller [12]). The extent of this spreading of sound energy is defined by an input parameter given for each surface, called the diffusion coefficient, which describes the proportion of rays (and, therefore energy) that is reflected diffusely; the rest is reflected specularly.

4.2 Limitations of RAYCUB

The original RAYCUB code, in Fortran, and its later modifications, permit the user to predict SPLs for various room dimensions and boundary conditions. Unfortunately, its accuracy is detrimentally affected by many oversimplifications, and by ignoring physical phenomena which occur in real sound fields. In particular, RAYCUB, a model which tracks the energy of received rays, and not their complex pressure, is unable to account for phase effects. It also does not predict sound intensity.

4.3 Program modifications

As previously stated, RAYCUB, with its previous upgrades, provides the user with a useful tool capable of predicting many room acoustical quantities that better able one to design rooms such as studios, offices, factories, classrooms, and other learning environments. Unfortunately, due to its simple implementation, results for rooms that include non-absorptive surfaces which have complex reflection coefficients are poor. Sound fields generally decrease with distance only, nodal patterns in the sound field are completely absent. Alleviation of these shortfalls would greatly improve the accuracy of the prediction as well as better the application opportunities. This was the objective of the new model named ORAYCUB.

4.4 Complex pressure

In RAYCUB, which assumes omni-directional sources, each ray is assigned a starting power such that the sum of the powers of the rays corresponds to the sound power level L_w of the source:

$$10\log\left(\sum W_{ray}\right) = L_{Wsource} \tag{4.1}$$

This results in each ray having real energy (pressure squared) properties, which can only be attenuated by real reflection coefficients. The power of each received ray is always summed, effectively ignoring phase.

ORAYCUB instead tracks the complex pressure of each ray. Similar to RAYCUB, the user-defined sound-source power level is equally divided amongst all the rays such that the sum of the squares of their pressures corresponds to the source power output as in Eq. (4.2); however, as the ray propagates it is assigned a phase.

$$10\log\frac{\sum P^2}{4e^{-10}} = L_{Wsource} \tag{4.2}$$

In order to define the starting pressure amplitude of the rays, it is necessary to find a value such that the square of the sum of the ray pressures relates to the sound-source power level defined by the user. The original ray power is:

$$W_{ray} = \frac{W}{N} \tag{4.3}$$

where W is the total source power, and N is the total number of rays. In the original program,

$$SPL = \sum \frac{W_{ray}}{N\,V} D\,\mathrm{e}^{iHR_{ray}} \tag{4.4}$$

where V is the volume of the receiver cell, D is the distance each ray travels through the receiver cell, H is the frequency-dependent air-absorption coefficient, and R_{ray} is the path length traveled by the ray from the source to the receiver.

In an anechoic environment, sound-pressure levels predicted by the new pressure model, with phase, should not differ from the original energy model. Therefore, in the

new pressure model, it was necessary to find a starting pressure amplitude X such that:

$$(X \cdot n)^2 = \frac{W}{N V} D n = SPL \tag{4.5}$$

where n is the number of rays received. Solving for X gives:

$$X = \frac{\sqrt{W D}}{\sqrt{V N n}} \tag{4.6}$$

In a free field, the expected ratio of the number of rays received to rays emitted is known:

$$\frac{n}{N} = \frac{L^2}{4 \pi R_{ray}^2} \tag{4.7}$$

where L is the cell side-length, from which the solution for n can be substituted into Eq. (4.6) to find:

$$X = 2 R_{ray} \frac{\sqrt{W \pi D}}{N L \sqrt{V}} \tag{4.8}$$

This value of X, the starting pressure of each ray emitted, is calculated every time a ray is received. To this, an air-absorption term is added before summing its contribution to the previous pressure value for a particular receiver point.

4.5 Path-length differences

Since ORAYCUB assigns each ray a complex pressure, implementing interference effects due to path length differences was possible. When a ray crosses a receiver cell, its complex pressure is calculated, and added to the complex total pressure for that receiver. This is done by first attenuating the pressure amplitude due to the distance traveled (spherical spreading) and assigning to the pressure contribution a phase equal to the path length (PL) of the ray divided by its wavelength:

$$P_{ray} = P_o e^{i 2 \pi PL / \lambda} \tag{4.9}$$

where P_o is the reduced pressure amplitude due to spherical spreading. Each receiver location has a total complex pressure for each frequency of interest. The SPL is found by taking the square of the absolute value of the total complex pressure and converting this

to decibels after adding a diffuse-field contribution equal to the energy remaining in the rays after their user-defined number of trajectories.

$$P_{total} = \sum P_{ray} e^{i2\pi\, PL/\lambda} \tag{4.10}$$

$$P_{total}^2 = P_{total}{}^2 + P_{diffuse\,remainder}^2 \tag{4.11}$$

$$SPL = 10 \log P_{total}^2 \tag{4.12}$$

4.6 Surface reflection

In early versions of the ray tracing-program, the energy of rays was attenuated by multiplying a ray's energy by the real reflection coefficient of each surface encountered. In ORAYCUB, complex pressure is tracked and is multiplied by the complex reflection coefficient of a surface, thereby accounting for phase shift on reflection. In ORAYCUB, this phase shift is added to the phase calculated due to path length. With every reflection, the pressure amplitude is attenuated and the additional phase change is accounted for. The phase shift of a surface is calculated from its complex reflection coefficient:

$$Phase\,Shift_{surface} = \arctan \frac{imag[RC_{surface}]}{real[RC_{surface}]} \tag{4.13}$$

This value is added to the total sum of all previous phase delays encountered by the ray:

$$Phase\,Shift_{total} = \sum Phase\,shift_{surface} \tag{4.14}$$

which is included when adding a ray's pressure contribution to a receiver location:

$$P_{total} = P_o e^{i(2\pi\, PL/\lambda + Phase\,shift_{total})} \tag{4.15}$$

4.7 Reflection coefficients

As discussed in Section 2.4, the surface impedance, and therefore the reflection and absorption coefficients, of many surfaces are dependent on the angle of incidence of the incident sound wave (extended reaction) (De Geetere [1]). Modeling this behaviour in the new model would be expected to increase the accuracy of prediction, when compared with experiment. Unfortunately, measurement techniques available to measure angularly-varying coefficients for use in prediction provide the user with a discrete set of impedance values measured at particular angles, which would not completely cover the infinite number of possible angles of incidence likely to be required in the prediction process. Angularly-varying reflection coefficients could be implemented in the model in two ways, the first by using the discretely known RC for the angle of incidence nearest the required one, or by interpolating an RC value between the known RCs. The better option would depend on the number of discrete RCs known, and whether the reflection coefficient variation with angle was linear. In the end, the use of variable reflection coefficients was not implemented in this work because an angle of incidence dependence was not measured (see Section 6.1).

4.8 Predicting sound-intensity levels

All prior modifications to RAYCUB discussed above had the objective of improving the accuracy of the sound-pressure level prediction model. Although RAYCUB already predicts many useful predicted values, an important one, sound intensity, is not included. ORAYCUB was extended to predict sound-intensity levels. In Section 2.4, sound intensity was defined as the product of sound pressure and particle velocity. Sound-intensity levels are predicted in ORAYCUB in two ways. One calculates the total, steady-state intensity vector that is the result of continuous noise generation. The other predicts the transient intensity response of received rays, their intensity values, and their direction of propagation, allowing the user to investigate the progression of energy flow resulting from an impulsive noise source. The new model does not predict particle velocity, it assumes that particle velocity is equal to sound

pressure/$\rho_o c$, and therefore, that the sound-intensity level is equal to $P^2/\rho_o c$. This assumption is valid for planar pure tone sound waves.

The steady-state intensity level, defined by three orthogonal components, is found by cumulatively summing the three components of all received rays. This process is normalized such that the pressure at the receiver is equivalent to the total received ray pressure. The final intensity vector is reported as a total sound-intensity level (SIL) and its three orthogonal components:

$$\vec{I}_{total} = \frac{\left(\sum_{rays} P_{i_{ray}}\hat{i} + P_{j_{ray}}\hat{j} + P_{k_{ray}}\hat{k}\right)^2}{p_o c} \tag{4.16}$$

The predicted transient intensity is calculated in a similar way, but the resultant intensity level and direction are calculated and recorded as a function of arrival time, saving resultant intensity vectors in bins. The resolution or sampling frequency is user defined, the result being an intensity echogram, the "I-echogram" where the variation with arrival time of sound-intensity level along with its directional components, rather than sound-pressure level, is recorded:

$$\vec{I}_{(L,U)} = \sum_{t\in(L,U)} W_i(t)\hat{i} + W_j(t)\hat{j} + W_k(t)\hat{k} \tag{4.17}$$

where L is the lower time boundary of the bin, and U is the upper time boundary equal to L + 1/sampling frequency.

Chapter 5

Validating the new ray-tracing program

Prior to the comparison of predicted and measured results, many validation cases were tested in order to identify implementation errors, or incorrectly modeled physics. These tests were conducted in such a way that theoretically correct results were easy to calculate, their complexities gradually increasing with each successful prediction. First let us consider how to ensure high prediction accuracy.

5.1 Prediction accuracy

ORAYCUB, like any numerical prediction model, suffers a trade off between model accuracy and computational cost, or "run time". Parameters that greatly influence the prediction accuracy are the number of rays emitted from the source, the number of trajectories or reflections tracked for each ray, and the number of receiver locations. Increasing any or all of these parameters can greatly increase the model accuracy, but each would result in a much higher computational cost. It is of utmost importance that a sufficient number of rays, and of reflections, as well as a sufficiently large number of receiver locations of sufficiently small volume, are used, in order to produce results that model the physics of the sound environment with sufficient accuracy since ORAYCUB is a numerical model and uses a statistical process. The following is an outline of the attempts made to investigate how the quantity of rays, trajectories, receivers, and the receiver-cell size affect prediction accuracy.

Table 5.1: Relationship between computational cost and accuracy in an anechoic environment.

Receiver cell side length	# of Rays (x10000)	Difference in predicted SPL(dB)	Computational time (s)
25 cm	1	3.8	4.5
25 cm	10	0.7	43.9
25 cm	100	0.3	442.8
10 cm	1	6.9	4.9
10 cm	10	2.8	48.1
10 cm	1000	0.7	485.1
5 cm	1	> 50	5.1
5 cm	10	9.2	51.7
5 cm	1000	3.7	516.6
5 cm	10000	0.5	4500
2 cm	10000	1.3	4800

The first test of the dependence of model accuracy on user-input parameters was to predict the sound field in a 4 x 4 x 4 m anechoic environment with a source emitting 200 Hz at its centre, by defining the room with six surfaces with reflection coefficients of zero. The model was used to find the number of rays and the cell size necessary to produce similar (within 1 dB) sound-pressure levels in all four corners of a plane at the same height as the source. Symmetry dictates that these levels should, in fact, be equal. Since the room is anechoic, this test removes the dependence of the predicted levels on the number of trajectories traced. Table 5.1 summarizes the prediction parameters, the difference between the lowest and highest predicted SPL, and the run time for each setup.

The results shown in Table 5.1 are not surprising. A receiver grid divided into smaller cells results in a greater number of receiver locations. Therefore, it is clear in column 4 that the prediction run time increases slightly with an increase in the total number of receiver locations within the sound field for the same number of rays traced. Also evident is the fact that smaller, more accurate receiver volumes require more rays, and much greater run times, in order to produce repeatable results. For example, tracking 100 000 rays is sufficient to predict SPLs within 1 dB for a receiver-cell side-length of 25 cm, but 1 million and 10 million rays are necessary to achieve a similar accuracy for side lengths of 10 and 5 cm, respectively. In this case, 10 million rays were not sufficient to produce results repeatable within 1 dB if the cell side length was 2 cm. As these are run times and accuracies predicted for a small, anechoic chamber, the effect of the number of rays and of receiver-cell size would be even more apparent in a larger room or one with reflecting surfaces.

Chapter 5

A second investigation was undertaken in order to characterize the effect of receiver-cell size has on prediction accuracy. In a room with reflecting surfaces, or in front of a single reflecting surface, the sound field demonstrates modal responses when reflected sound waves interfere with each other. It is necessary to predict such sound fields using a receiver volume small enough that interference effects do not vary greatly across it, in order to prevent the averaging of either constructive or destructive interference effects. For example, failing to use a small enough receiver volume would result in room nodes being underestimated by the prediction model. The test configuration involved a single sound source located 3 m from a single reflecting plane in an otherwise anechoic environment. The reflecting surface was given an infinite impedance; therefore it had a reflection coefficient of 1. The sound-pressure level was predicted on an array of receivers between a 100 dB source and the reflecting plane, using various cell side-lengths and numbers of rays. Since only one surface was involved, this test also removed the prediction dependence on the number of tracked trajectories, since only one reflection could result in a sound wave interfering with the direct sound field. The results comparing theory and prediction, using side lengths of 10, 5 and 1 cm and 100 000 to 10 million rays, are shown in Figs. 5.1, 5.2 and 5.3.

It is evident in Figs. 5.1 to 5.3 that the number of rays required for accurate prediction increases greatly with decreasing receiver volume. In fact, 10 million rays were not sufficient if the receiver volume had a side length of 1 cm. Also apparent is the fact that, in the case where only one reflecting surface is present, a 5cm receiver side-length is small enough to very accurately model the sound field. For this reason, a receiver side length of 5 cm, and 1 000 000 rays were used for all subsequent work that included one or more reflecting surfaces.

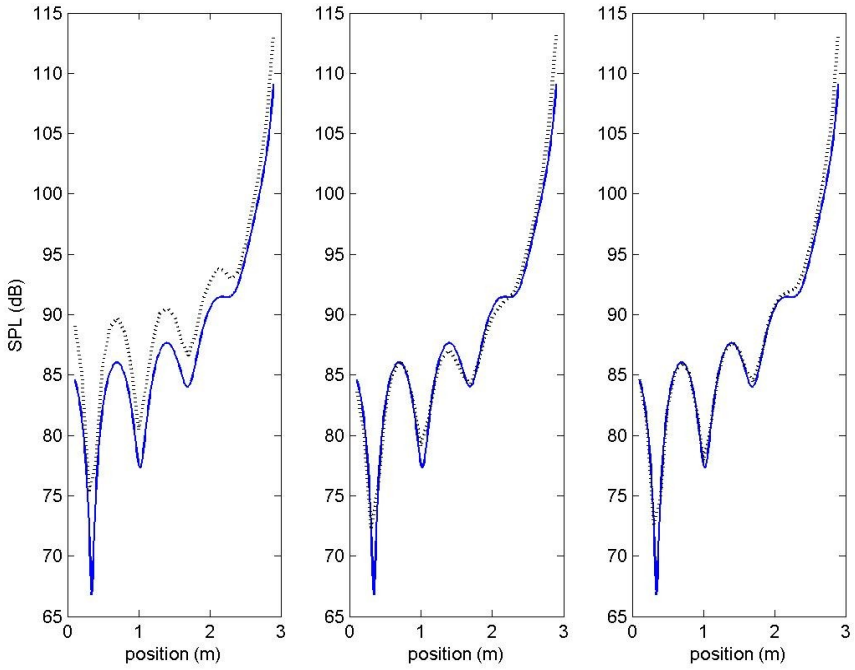

Figure 5.1: SPLs between a source and a wall of infinite impedance using a cell dimension of 10 cm, and 100 000 (left), 1 million (centre), and 10 million (right) rays (- theory, -- predicted).

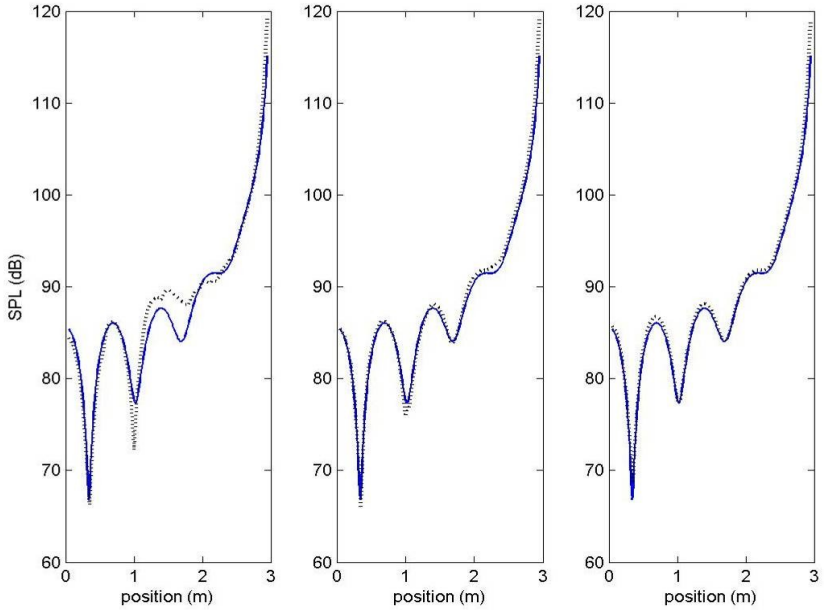

Figure 5.2: SPLs between a source and a wall of infinite impedance using a cell dimension of 5 cm and 100 000 (left), 1 million (centre), and 10 million (right) rays (- theory, -- predicted).

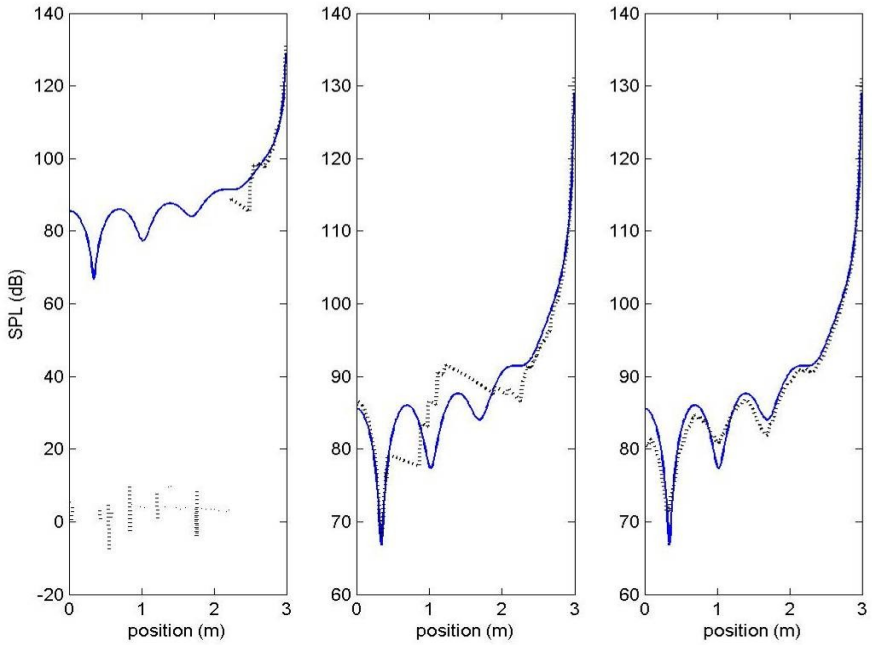

Figure 5.3: SPLs between a source and a wall of infinite impedance using a cell dimension of 1 cm and 100 000 (left), 1 million (centre), 10 million (right) rays (- theory, -- predicted).

5.2 Phase effects due to path length

The first validation test compared the sound-pressure levels at grid receiver positions on a plane in an anechoic room, with a source in the centre. Theoretically, the SPLs calculated including the phase implementation should be the same as those predicted using the original model since, without reflection, there are no secondary paths which can interfere with the direct path. Figures 5.4 and 5.5 show the sound field predicted with and without phase effects, respectively, for a 4 x 4 x 4 m^3 room with the source at the centre, with a spacing interval of 10 cm.

The comparison of the graphs leads to three conclusions. They are:

- The fact that both sound fields are identical demonstrates that interference is not occurring, as it cannot in an anechoic chamber, suggesting correct implementation;

- The original code has been correctly translated into MATLAB, since a doubling of distance from the source results in a reduction of 6 dB in both graphs.

- The characteristic of the original program, giving incorrect results for any cell that contains a source, is still evident in the results predicted using the newer version. In Figs. 5.4 and 5.5, this is evident by the unrealistically high levels at the room centre.

The next validation test was to predict SPLs between two identical sources in an anechoic environment. One would expect a standing-wave pattern to be evident, where the number of nodes, located at intervals of λ apart, increases with frequency. This is theoretically the case, since positions that are out of phase reoccur every 2π in phase, corresponding to a wavelength apart. In Fig. 5.6 are the results for two sources, with equal power levels of 100 dB, in phase, separated by 2 m, for the frequencies of 125, 250, and 500 Hz. Also shown are the theoretical results.

These results further suggest the correct implementation of the interference due to path-length differences. They also demonstrate the drawback of a ray-tracing program, that perfect constructive or perfect destructive interference is impossible to model due to the necessity of defining a receiver with non-zero, not infinitesimal, volume. All plots should be symmetrical about the 1 m position; any asymmetry is the result of the randomness of the ray generator for each source. Please refer to Section 5.1 for the investigation of the trade-off between computational cost and model accuracy.

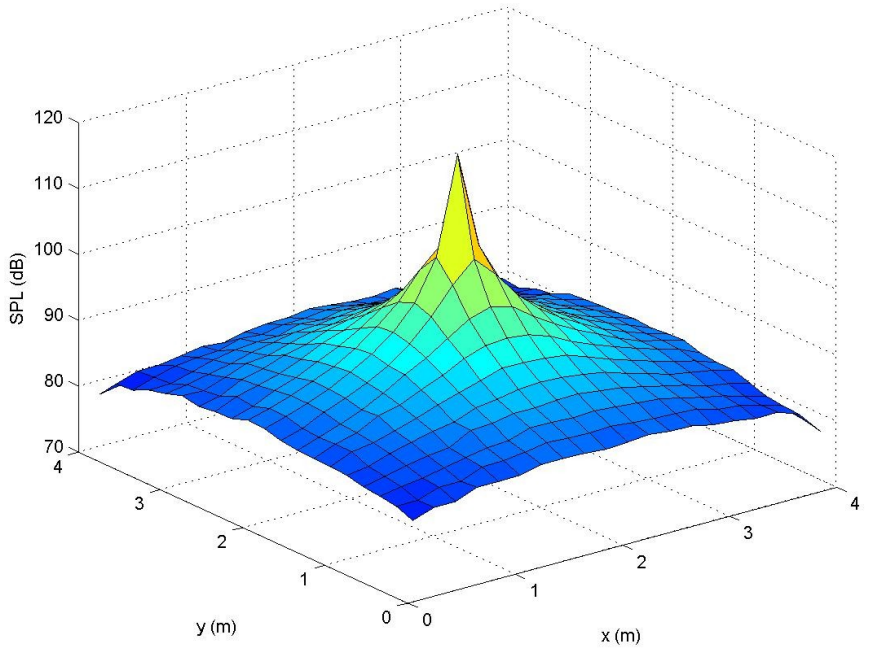

Figure 5.4: Sound field in an anechoic room, predicted by ray tracing without phase effects.

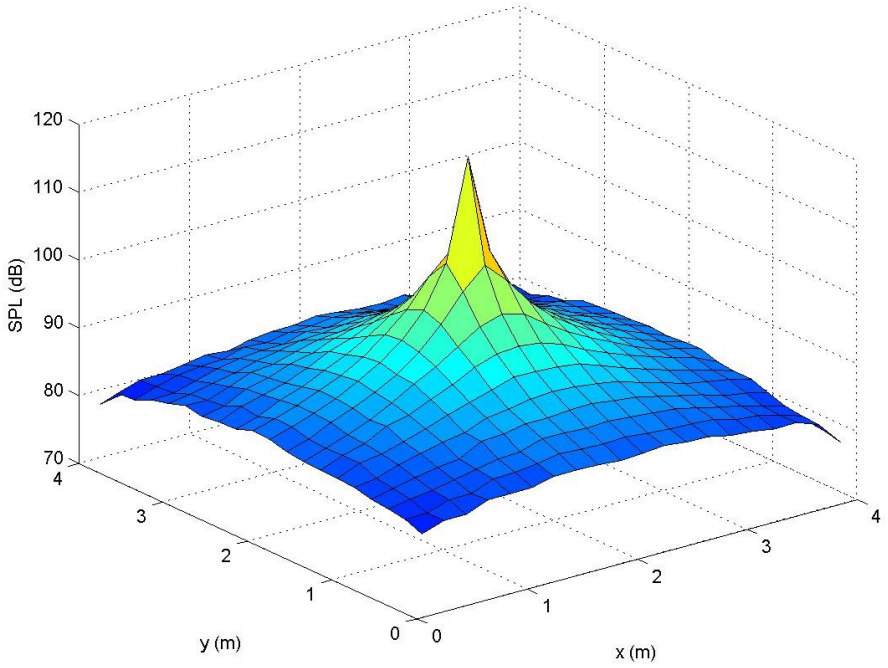

Figure 5.5: Sound field in an anechoic room, predicted by ray tracing with phase effects.

The correct modeling of the physics of these phenomena was confirmed by predicting the SPLs on an array of receiver locations between a source (sound power level = 100 dB) and a single reflecting 4 x 4 m wall of infinite impedance in the anechoic chamber. In the absence of other reflective surfaces, one would expect the SPL to decrease with distance from the source, and to include a node where the reflected wave is 180^{o} out of phase with the direct sound. This occurs at a distance of ¼ wavelength from a surface of infinite impedance, since the reflected wave travels this distance twice, equaling ½ wavelength. In Fig. 5.7 are the ray-tracing predicted results for a source located 3 m from a 4 x 4 m reflecting surface with RC = 1, located at x=0, and the theoretical results.

The graphs show some interesting features. Obvious is the fact that the node position is increasingly closer to the partition as the frequency increases, as theory predicts, since the wavelength of the sound wave is decreasing, further proof of correct implementation. Another feature to note is that, in all cases, sound-pressure levels near the reflecting surfaces are predicted to be lower than theory would suggest. The reason for this may be that the number of rays used was insufficient to ensure statistical accuracy at greater distances from the source. Due to spherical spreading, receivers which are further from a source receive fewer rays, and therefore require more rays to be emitted for good prediction accuracy. This hypothesis is supported in Figs. 5.1 to 5.3 in Section 5.1. In these figures it is obvious that prediction accuracy near reflecting surfaces, far from a source, require a very large number of rays for a receiver volume of 5 cm. Another interesting feature is that more than one node is obvious in Fig. 5.7; these occur every half wavelength, where the reflected wave is again 180^{o} out of phase. The nodes farther from the partition have a smaller reduction in amplitude since the amplitude of the reflected wave is much less than that of the direct wave. As previously stated, RAYCUB does not account for phase, this fact is clear in Fig. 5.7 where the SPLs predicted using RAYCUB simply attenuate with distance from the source without including any nodes.

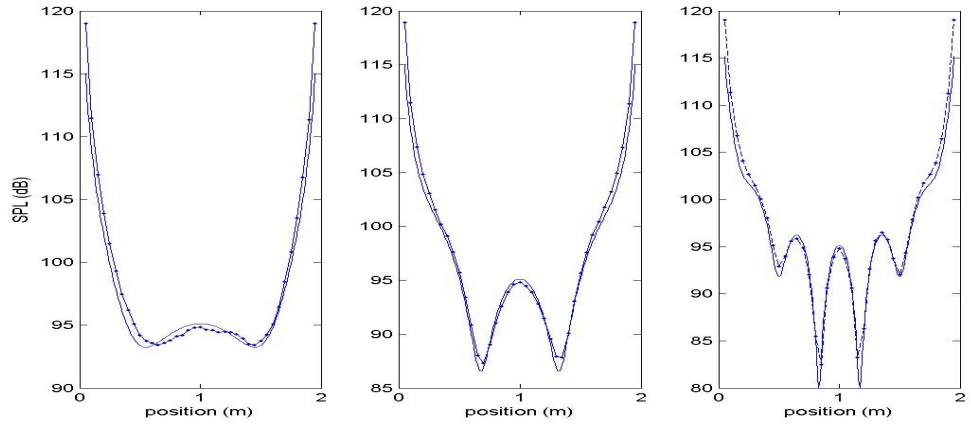

Figure 5.6: Ray-tracing predicted (—●—) and theoretical (——) SPLs between two identical sources, at 125 Hz (left), 250 Hz (centre), and 500 Hz (right).

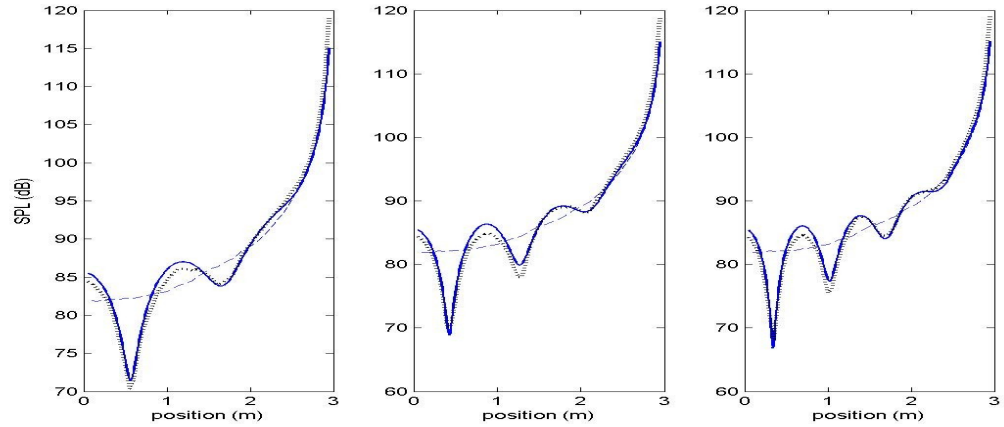

Figure 5.7: ORAYCUB predicted (····) theoretical (▬) and predicted using RAYCUB (- - -) SPLs between a source and reflecting plane, at 150 (left), 200 (centre), and 250 Hz (right).

5.3 Surfaces with non-infinite impedance

The original RAYCUB program has previously been validated using real reflection coefficients in energetic terms. A simple test case was run, using various complex RCs, to test whether or not the physics was modeled and implemented correctly. As in Section 5.1, SPLs were predicted between a source and a single 4 m x 4 m panel, which now had a complex RC. The phase delay imparted to the reflected wave should be recognizable by a shift in the nodal locations. Fig. 5.8 shows the results for a source of power level 100 dB, 3 m from a surface, comparing the SPLs with RCs of 1 and 0.85 + 0.004i.

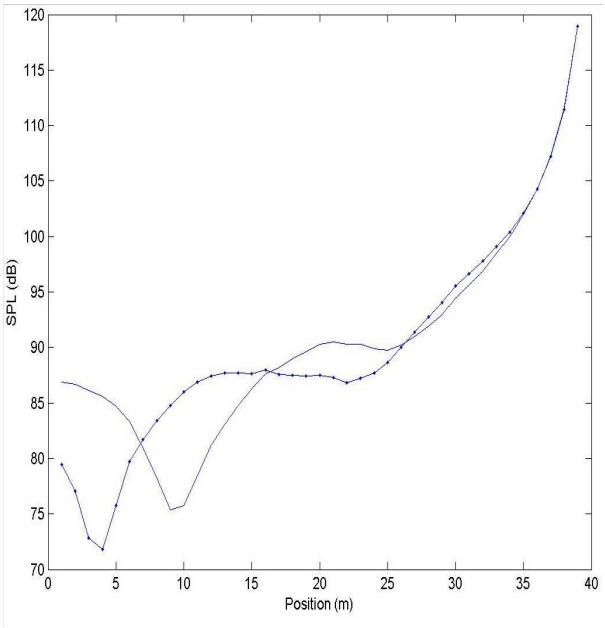

Figure 5.8: Ray-tracing predicted SPLs between a source and reflecting plane (— = rigid surface, —●— = surface of non-infinite impedance), at 175 Hz.

As the plot suggests, ORAYCUB correctly models the effect of a complex RC, since the distance by which the node is shifted is representative of the phase change. Also noteworthy is the reduction in pressure levels near the plane due to a reduction in the magnitude of the RC.

5.4 Steady-state intensity

Validation of the prediction of the intensity vector first involved finding the intensity levels at two receiver locations in an anechoic room. Theory suggests that the vectors should point directly away from the source, and have an SIL equal to the SPL. Fig. 5.9 displays the floor plan of the test environment. Fig. 5.10 and 5.11 are 2D compass plots showing the measured and predicted directions of the intensity vector in each plane, for a 4 x 4 x 4 m room, confirming this.

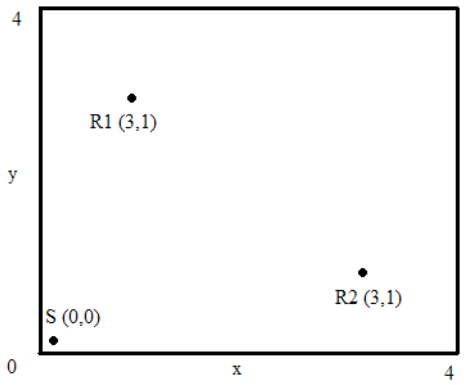

Figure 5.9: Floor plan of source and receiver locations.

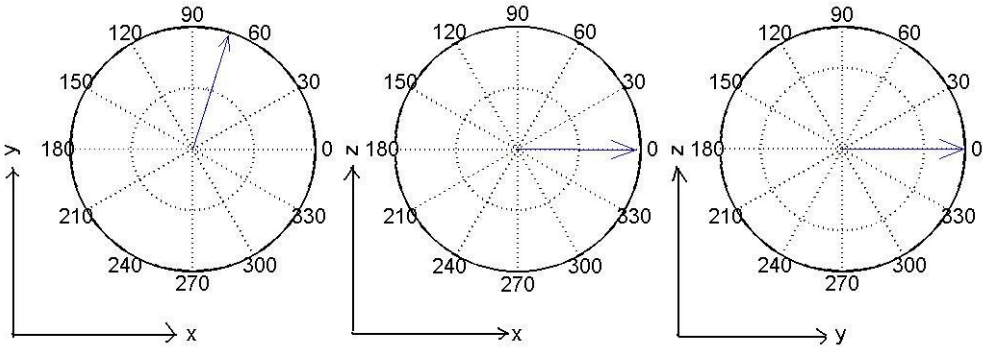

Figure 5.10: 2D plots of the sound intensity direction for receiver location 1.

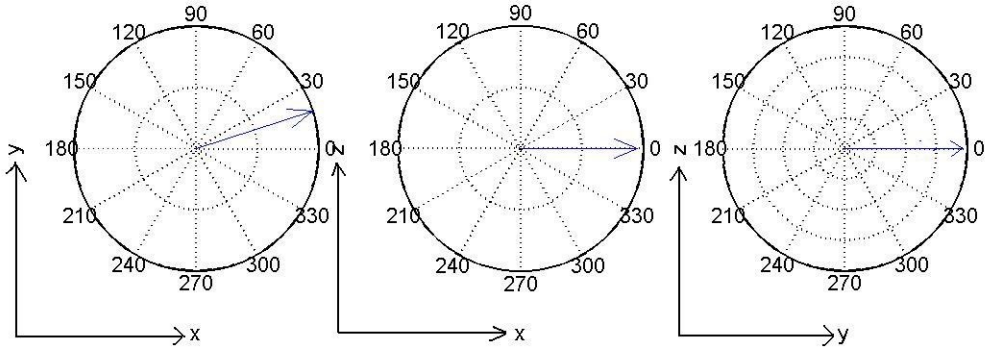

Figure 5.11: 2D plots of the sound intensity direction for receiver location 2.

Total sound-intensity levels were 78.0 and 78.5 dB at locations 1 and 2, respectively. These predictions were made with both receivers at the same height as the source, explaining the lack of a z component for both intensities.

Another validation test involved investigating whether the sound intensity between two sources was significantly less than the predicted SPL, since, in this case, all components of the intensity from one source are canceled by the intensity of the other source. In a test where the sources were 2 m apart, with equal power outputs, the predicted SPL was 81 dB while the SIL was 65 dB. The 16 dB difference is less than theory would suggest, due to the randomness of the ray-tracing algorithm and the non-zero receiver size, but significant enough to suggest proper implementation.

This was further investigated by moving the receiver off axis, but still located between the sources, the locations as shown in Fig. 5.12.

The predicted SIL was 74 dB while the SPL was 77 dB. The difference between the two levels is less since, in this case, only two of the three components of sound intensity are canceled. The 2D direction of the resultant intensity is shown in Fig. 5.13.

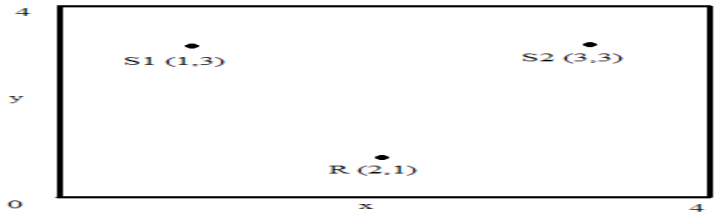

Figure 5.12: Floor plan depicting locations of sources and receiver location.

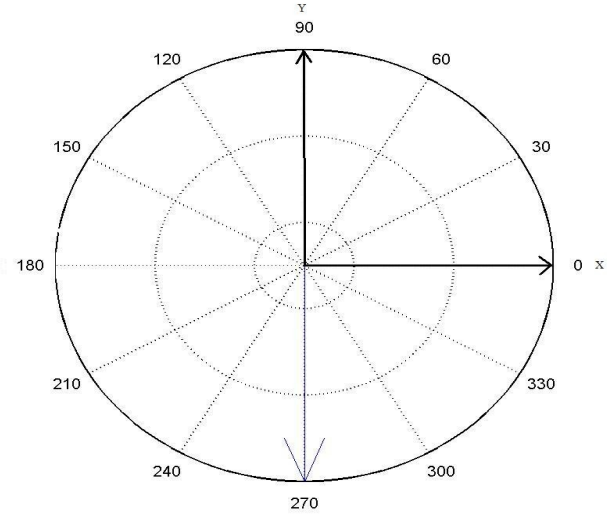

Figure 5.13: Ray-tracing predicted sound intensity direction for receiver as shown in Fig. 5.12.

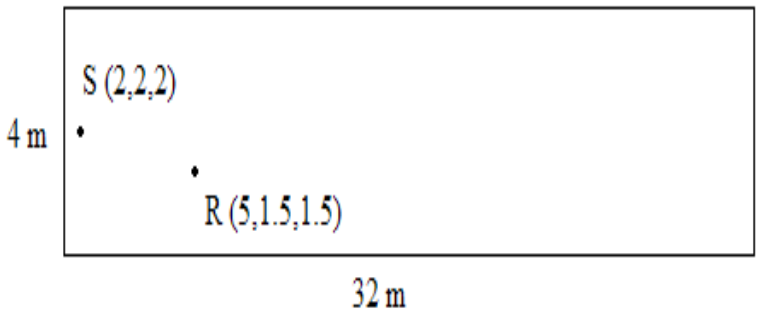

Figure 5.14: Floor plan of large room with diffusely reflecting surfaces, showing the source and receiver locations.

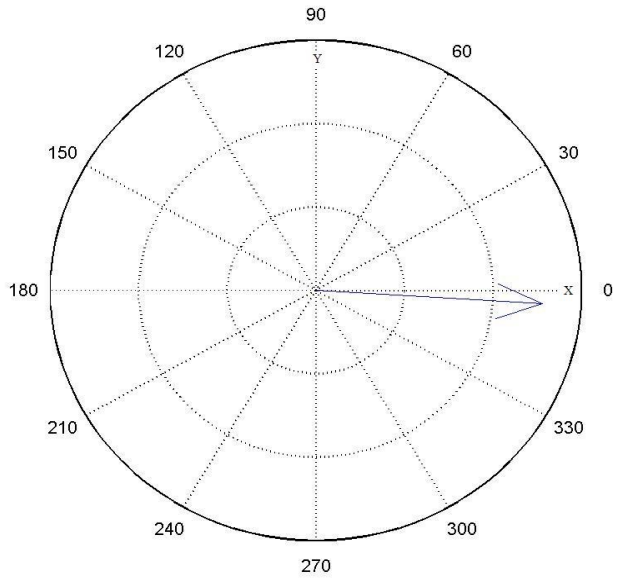

Figure 5.15: Sound-intensity direction as predicted by ray tracing for the room shown in Fig. 5.11.

A final test involved predicting the intensity level at one point in a room which has surfaces that are all highly reflective (RC = 0.99), and have a large diffusion coefficient (0.9). Fig. 5.15 is a plot of the intensity vector at the point (5, 1.5, 1.5) in a large room of dimensions 32 x 4 x 4 m^3. A single source was located at (2, 2, 2) as shown in Fig. 5.14.

Fig. 5.15 shows an intensity vector pointing directly away from the source at (2, 2, 2). This agrees well with theory, since the boundary conditions of the environment would create a highly diffuse sound field (Kutruff [2]). In this diffuse (reverberant)

sound field, the only sound wave that does not have an effective "mirror source" defined by one of the multitudes of reflections would be the direct sound wave. This wave, the only one without components canceled, produces an intensity pointing away from the source, exactly as predicted.

5.5 Transient Intensity

To validate the implementation of the transient-intensity prediction, a single reflecting surface was considered. This intensity was found at a point near a 10 x 10 m^2 plane, as shown in Fig. 5.16.

The transient intensity at the receiver location R was predicted using a surface with a reflection coefficient of 1, and varying diffusion coefficients. Fig. 5.17 shows the results.

From the resulting intensity vectors, it is obvious that the implementation is distinguishing the difference in the number of received sound waves as a function of the diffusion coefficient of the surface. In the case of DC = 0, only two intensity vectors are present, representing the direct and specularly-reflected sound waves, in agreement with theory, since a DC of 0 implies that a surface reflects purely specularly.

The number of intensity vectors increases with the DC, which also agrees with theory, considering that a surface with a greater DC reflects sound away from the specular angle to a greater amount. Fewer rays were received from paths which reflected from points past the receiver (at x coordinates between 8 and 10 m) as shown in Fig. 5.17 because the time resolution causes the averaging of this path with those which reflect at angles closer to specular.

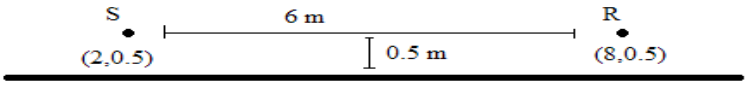

Figure 5.16: Schematic of prediction setup for transient-intensity validation

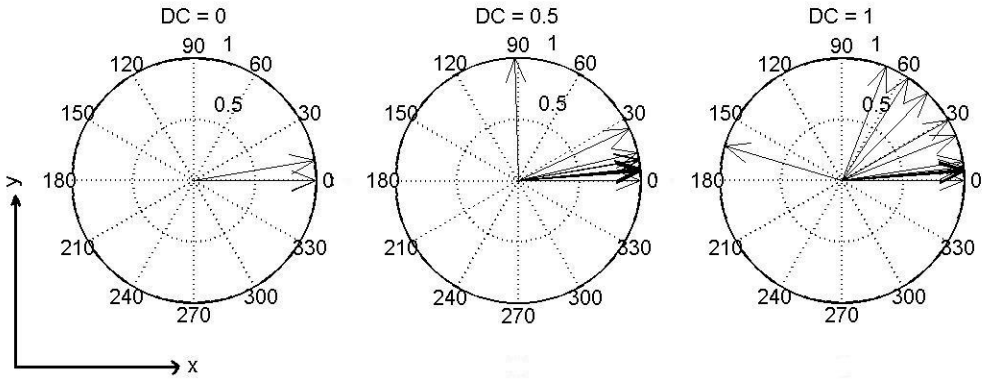

Figure 5.17: Transient sound-intensity directions for varying diffusion coefficients of 0 (left), 0.5 (centre) and 1 (right), respectively.

Chapter 6

Experimental comparison

Validation in comparison with theoretical prediction was only the first step in this work completed in an effort to evaluate the usefulness of ORAYCUB. When the modified program had satisfied validation, it was necessary to compare the predicted pressure and intensity levels with actual values measured in reflecting environments, the sixth research objective, as stated in Section 3.2. Analyzing the comparison results permitted objective conclusions about the program's overall effectiveness, the last research objective, to be made. Since prediction requires the input of complex surface RCs, predictions are only as accurate as the method with which those RCs are measured.

6.1 Measuring complex reflection coefficients

In order to compare predicted results with measured data, the boundary and source conditions need to be accurately defined in ORAYCUB. One such variable of importance is the complex reflection coefficients of the surfaces. These were measured using two methods, the first using an impedance tube, the second using the *spherical decoupling method* (SDM).

Calculating the complex impedance and, therefore, the complex reflection coefficient of a material by the two-microphone transfer-function method using an impedance tube is a well documented and validated procedure. For this reason, the details of the method will not be discussed in this work, but they can be found in the ASTM E1050-98 standard [13], upon which the results presented here are based. A previous implementation of this standard was used in this work, the results of which were assumed to be accurate. It allows one to measure a surface's specific acoustic resistance, specific acoustic reactance ratio, sound-absorption coefficient, etc. All results found using an impedance tube are valid for normal sound incidence only.

Four common materials found in rooms were measured in a B&K Type 4002 Impedance Tube, using a Norwegian Electronics RTA (Real Time Analyzer) Type 830.

The real and imaginary parts, as well as the magnitudes, of the (normal-incidence) reflection coefficients of 1/2" plywood, carpet, drywall, and acoustical ceiling tile are shown in Figs. 6.1 and 6.2. All samples were 10 cm disks rigidly backed by a 2 cm thick, stainless-steel sample holder. The impedance tube used had a theoretical frequency range of 50 to 2000 Hz. Results suggest that RCs at frequencies lower than 200 Hz are inaccurate.

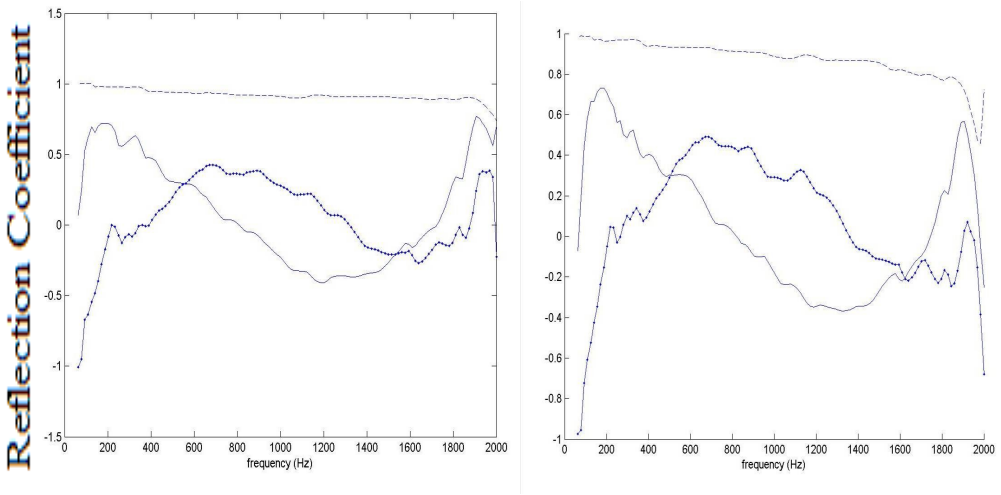

Figure 6.1: Measured reflection coefficients of plywood (left) and carpet (right) as found using the impedance tube (—— real part, —●— imaginary part, - - - magnitude).

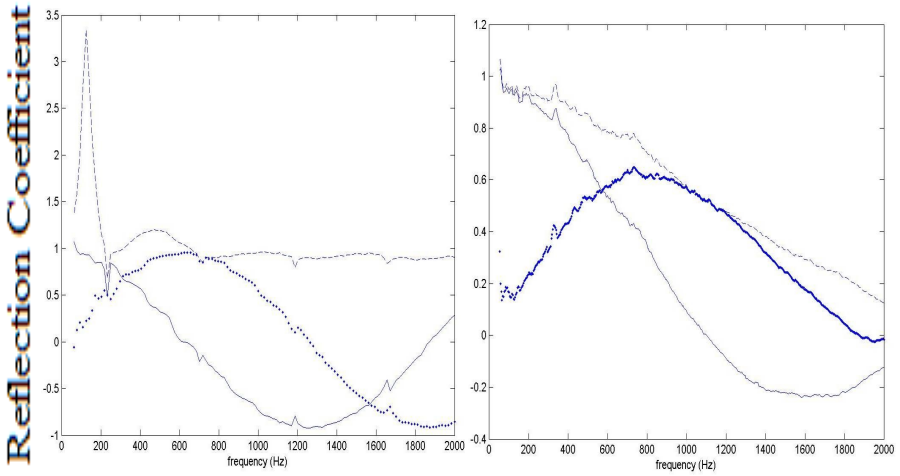

Figure 6.2: Measured reflection coefficients of drywall (left) and ceiling tile (right) as found using the impedance tube (—— real part, —●— imaginary part, - - - magnitude).

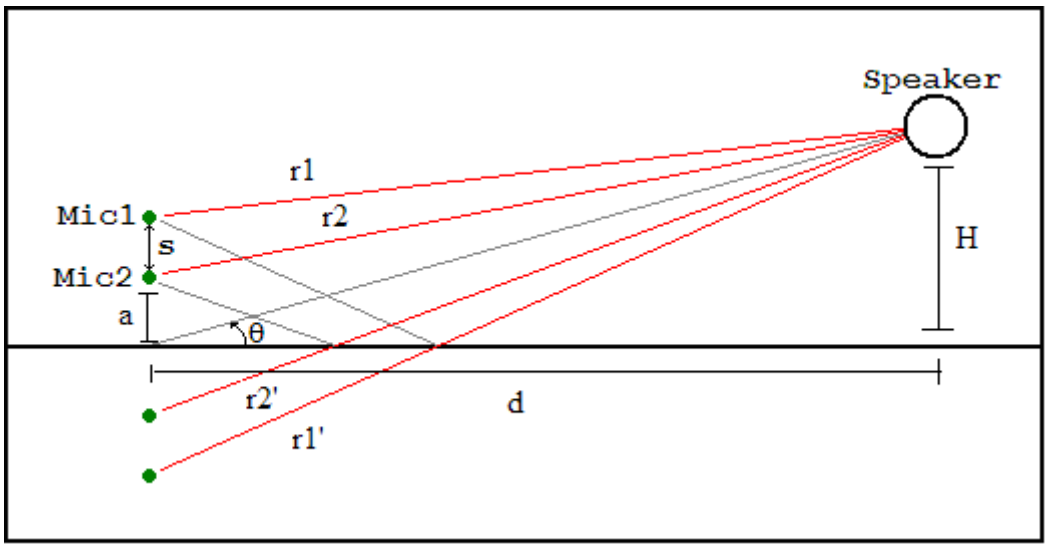

Figure 6.3: Schematic of experimental setup for the spherical-decoupling method.

Reflection coefficients were also measured in an anechoic chamber using the spherical-decoupling method (Champoux and Allard [14]). Unlike the impedance tube, it is possible to measure reflection coefficients at any angle of sound incidence. This is a two-microphone method, which uses the cross-spectrum of the complex pressure signals at the two microphone positions, and the mirror-image-source approximation, to find the complex impedance and complex reflection coefficient of the material being studied. The experimental setup is as in Fig. 6.3.

The pressures measured at microphones 1 and 2 are the sum of the direct and reflected waves:

$$P_1 = P_o[e^{ikr_1}/r_1 + Re^{ikr'_1}/r'_1] \tag{6.1}$$

$$P_2 = P_o[e^{ikr_2}/r_2 + Re^{ikr'_2}/r'_2] \tag{6.2}$$

where R is the reflection coefficient of the surface. The pressure amplitude can be eliminated by dividing the two equations:

$$H_{12} = P_1 / P_2 = \frac{e^{ikr_1}/r_1 + R\,e^{ikr'_1}/r'_1}{e^{ikr_2}/r_2 + R\,e^{ikr'_2}/r'_2} \tag{6.3}$$

Solving for R gives:

$$R = \frac{e^{ikr_1}/r_1 - H_{12}\,e^{ikr_2}/r_2}{e^{ikr'_1}/r'_1 - H_{12}\,e^{ikr'_2}/r'_2} \tag{6.4}$$

which is a complex value provided $H_{12} = P_1/P_2$ is measured as a complex quantity. The lengths of r'_1 and r'_2 can be shown to be:

$$r'_1 = \sqrt{d^2 + (H + a + s)^2} \tag{6.5}$$

$$r'_2 = \sqrt{d^2 + (H + a)^2} \tag{6.6}$$

The complex RCs for the same four materials (plywood, carpet, drywall, ceiling tile) were measured at normal incidence in order to compare their values with those found with the impedance tube. The plywood, carpet, drywall samples had dimensions of 2.44 m x 2.44 m, while the acoustical ceiling tile had dimensions of 1.22 m x 2.44 m. The carpet and ceiling tile samples were rigidly backed with 1 inch plywood. Figs. 6.4 and 6.5 show these results. Note that the frequency range of the spherical decoupling method is greater than the range of the impedance tube method.

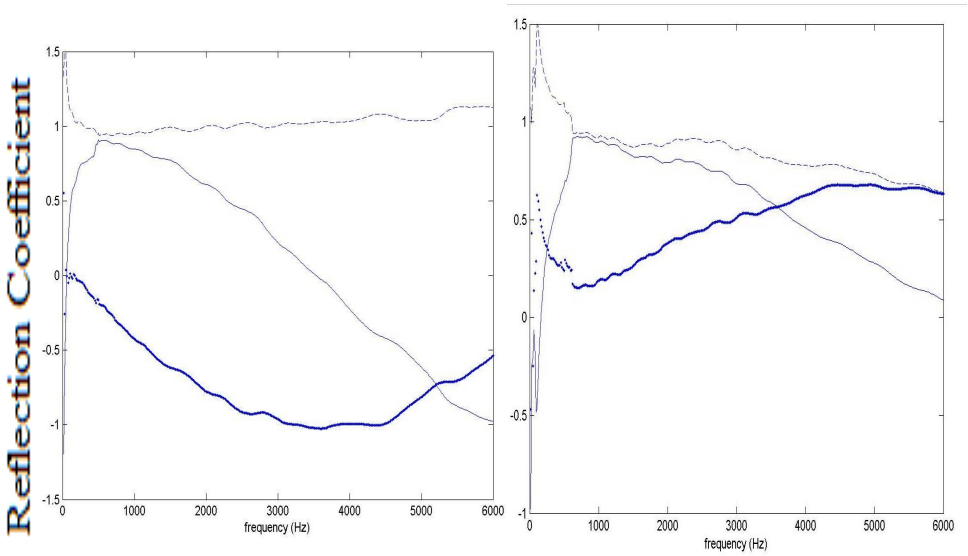

Figure 6.4: Measured reflection coefficients of plywood (left) and carpet (right) as found using the spherical-decoupling method (—— real part, ▬▬ imaginary part, ••• magnitude).

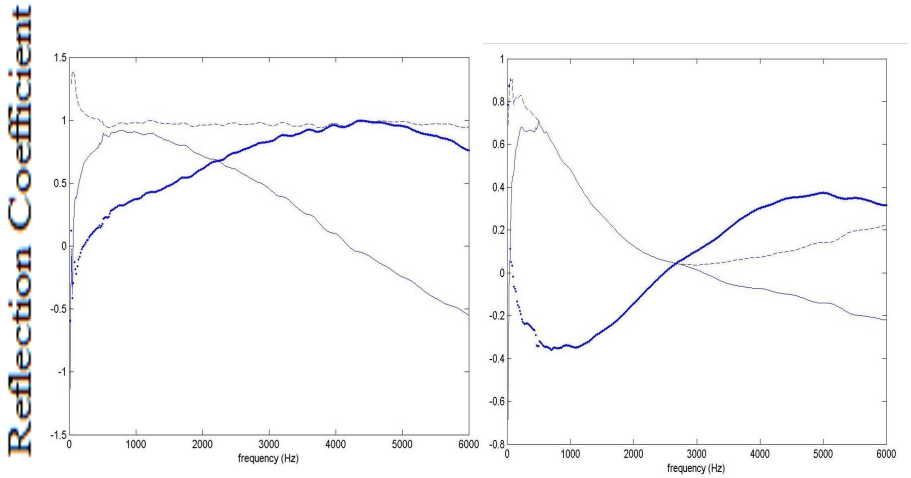

Figure 6.5: Measured reflection coefficients of drywall (left) and ceiling tile (right) as found using the spherical-decoupling method (—— real part, ▬▬ imaginary part, ••• magnitude).

Comparing the results found using the spherical-decoupling method and those found with the impedance tube, it was apparent that the two methods do not give similar complex reflection coefficients. The complex values of the RCs measured by the two methods differ. This may, in part, be due to the fact that the samples in the anechoic chamber were of sufficient size for lateral vibration and/or bending waves to occur. These samples were also backed with plywood, instead of stainless-steel as they were in

the impedance tube, therefore coupling the reflective properties of the sample and the underlying plywood. Samples for the spherical-decoupling method were large enough, and the microphones placed near enough to the sample (Mic 2 height of 3 cm above surface), to make edge-diffraction effects negligible.

It is much more likely that the complex reflection coefficients do not agree because the impedance tube method that was used calculated incorrect complex reflection coefficient values. This is clearly the case since the magnitude of the complex RCs is not equal to $1 - |R|^2$ as it should be. It does appear that the magnitudes of the reflection coefficients agree well but, as it was explained in Section 2.4, it is not only the magnitude of the RC, but the individual real and imaginary parts that affect the amplitude and phase of the reflected sound wave. Due to this fact, it was of interest to compare sound-pressure levels predicted using RC values found by both methods, in order to determine which was the most accurate.

In Section 2.4 it was explained that the impedances and corresponding reflection coefficients of many surfaces vary with angle of incidence. Implementing angle of incidence dependence into ORAYCUB would not be difficult, but it was first required to identify the characteristics of a few of these surfaces. This was done in order to understand how to best implement angle dependence such that prediction agrees with well experiment. This was necessary before deciding whether to interpolate a complex reflection coefficient from the known discrete values, or to use the known RC at the nearest angle of incidence. The impedance tube is not helpful in this case, since it only gives the impedance at normal sound incidence, but the spherical decoupling method is valid for any angle of incidence. Figs. 6.6 and 6.7 show the results for all the surfaces measured in the anechoic chamber, for angles of incidence of 34, 51, 55, and 90°.

Two things were concluded upon reviewing these results. First it appeared that there was no obvious linear relationship between angle of incidence, and the magnitude of the reflection coefficient. This meant that prediction would only be accurate provided a large number of discrete complex values of RC was known. On the basis of this, it was decided not to include angularly varying RCs in the program at all, in order to reduce the

complexity of running the program for the user. Therefore, the normal-incidence impedance values were used in all comparisons.

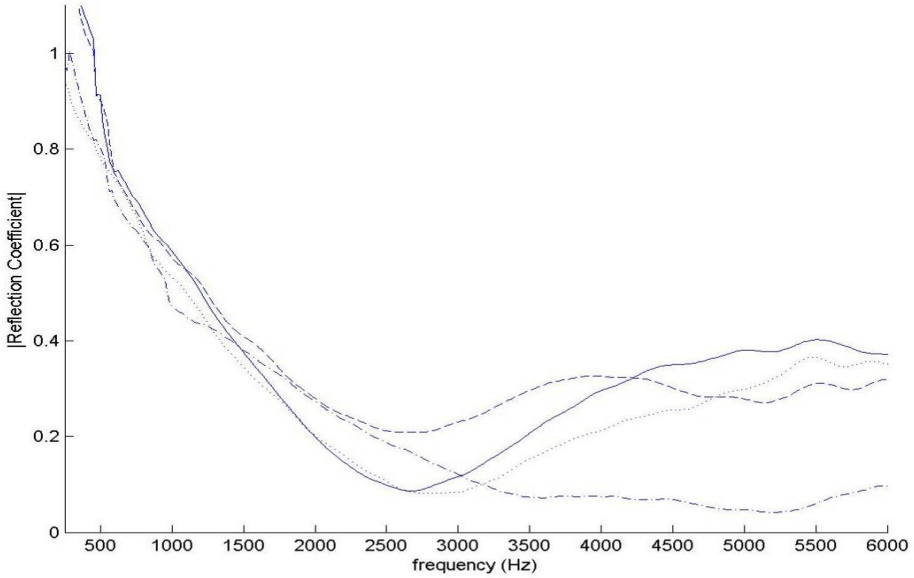

Figure 6.6: Measured reflection-coefficient magnitude of acoustical ceiling tile for multiple angles of incidence (—— = 90, ••• = 55, - - - = 51, —•— = 34 degrees).

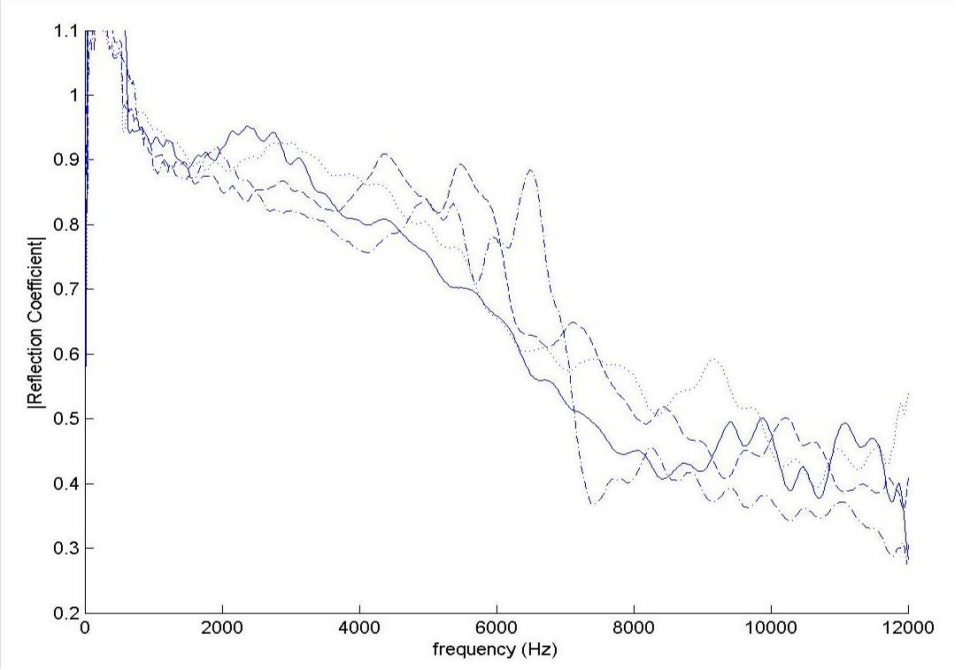

Figure 6.7: Measured reflection-coefficient magnitude of carpet for multiple angles of incidence (—— = 90, ••• = 55, - - - = 51, —•— = 34 degrees).

6.2 Single reflecting plane

The first of numerous experiments was to compare the measured and predicted SPLs, at an array of microphone positions between a source and a single reflecting plane in an anechoic chamber. This was first done at normal incidence as shown in Figs. 6.8 and 6.9.

This comparison was done for all four surfaces previously characterized in the impedance tube and using the spherical decoupling method at three frequencies, each an octave apart (250, 500, 1000 Hz). The source, an 8" loudspeaker, was suspended from the ceiling, with the sample on the floor approximately 2 m from the source (see Fig. 6.9). In order to prevent near-field effects in the vicinity of the source from affecting the results, the sound-pressure levels were measured in 10 cm increments from the surface to 1 m away from the surface. Figs. 6.10 to 6.13 show the measured values, the levels predicted by ORAYCUB using RCs measured by both the impedance tube and spherical decoupling method, and the levels predicted using a real RC equal to the magnitude of the complex RC.

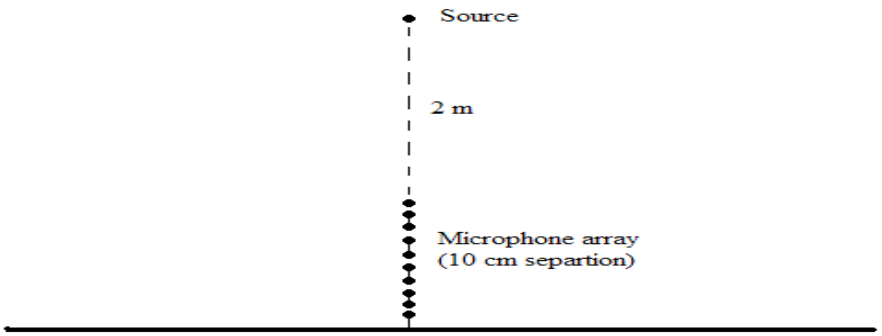

Figure 6.8: Schematic of experimental setup.

Figure 6.9: Photograph of measurement setup for SPLs over a single reflecting plane.

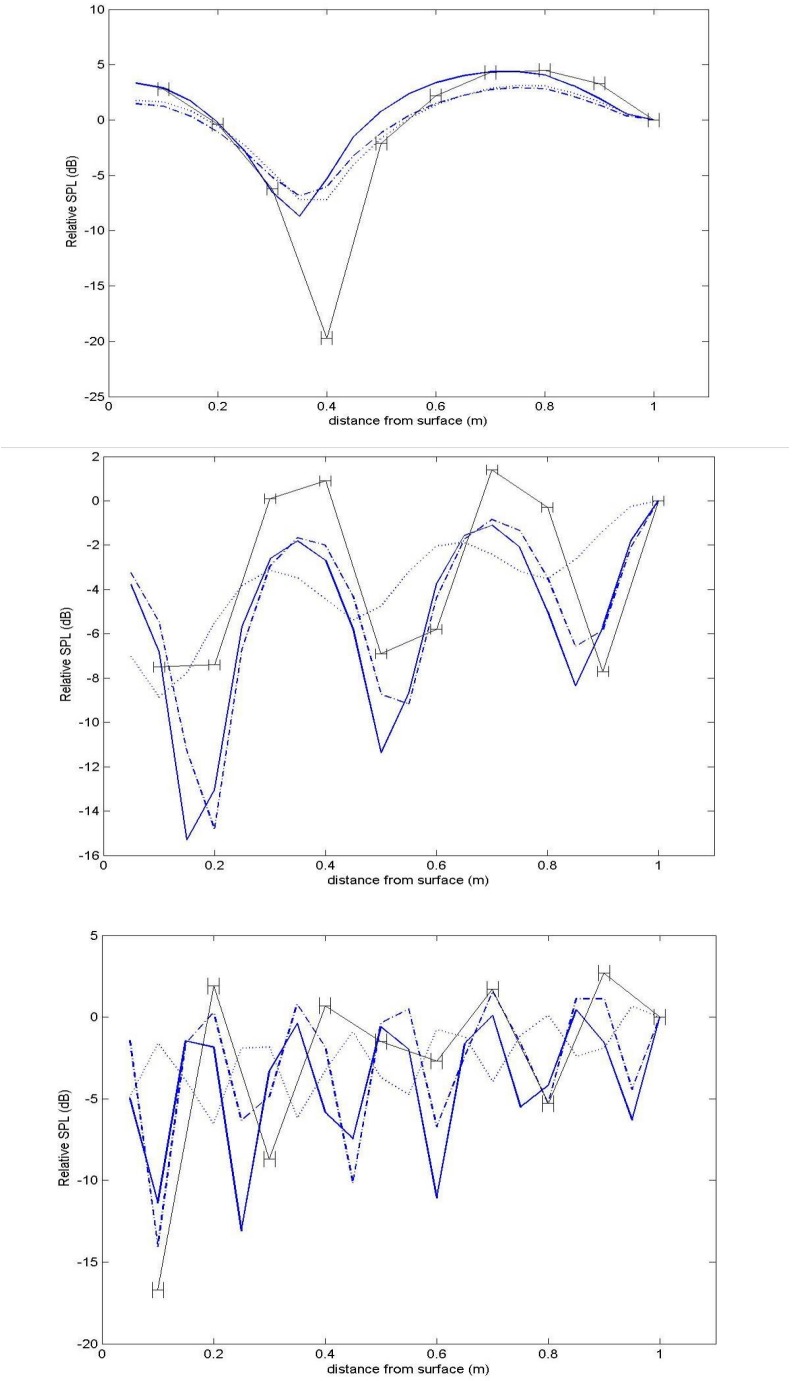

Figure 6.10: SPLs between a surface of plywood and a source, at 250 Hz (top), 500 Hz (middle), and 1000 Hz (bottom) (|-| = measured, ——= predicted, real RC, ••• = predicted, impedance tube RC, - - - = predicted, SDM RC).

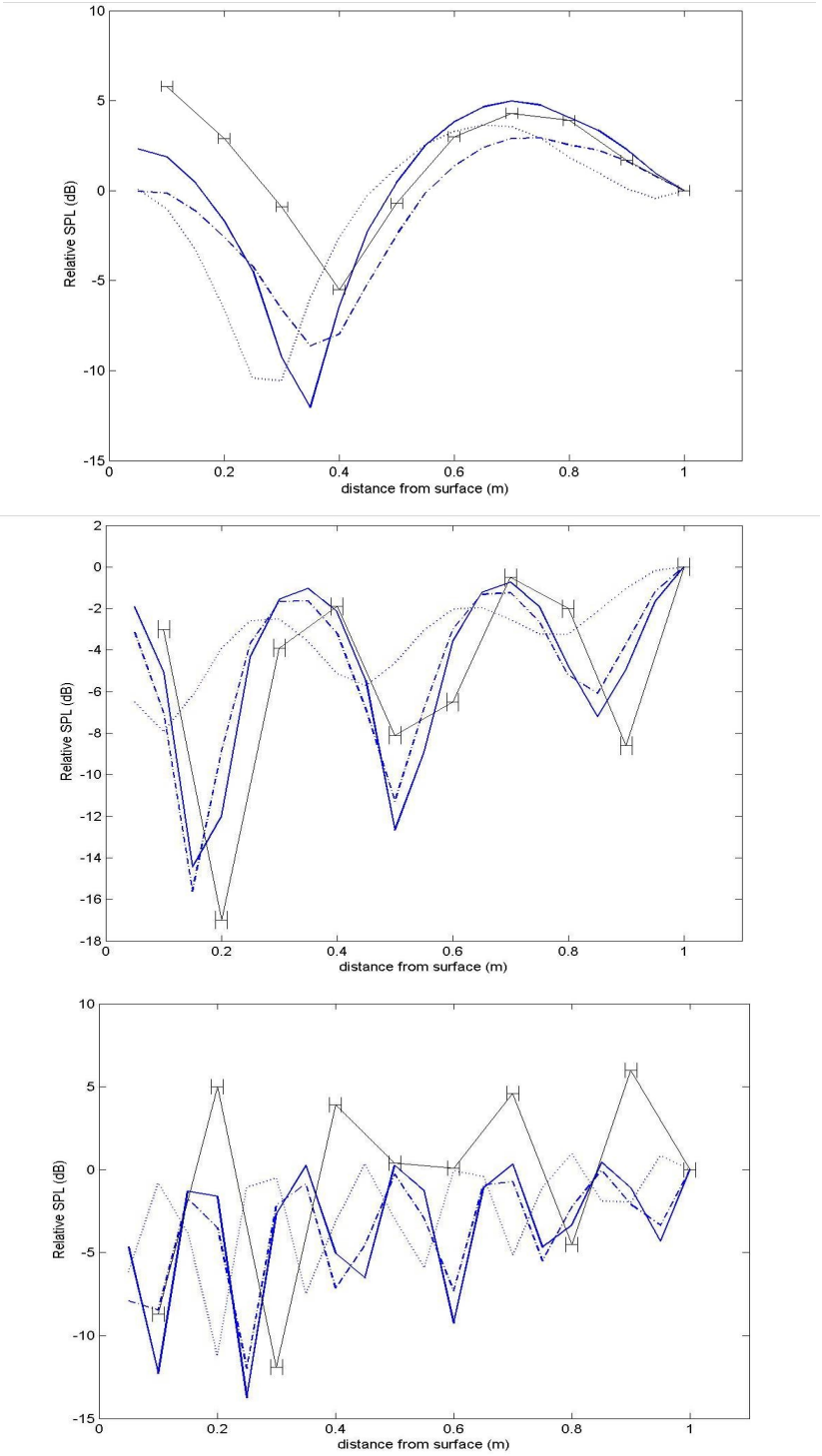

Figure 6.11: SPLs between a surface of drywall and a source, at 250 Hz (top), 500 Hz (middle), and 1000 Hz (bottom) (|-| = measured, —— = predicted, real RC, ••• = predicted, impedance tube RC, - - - = predicted, SDM RC).

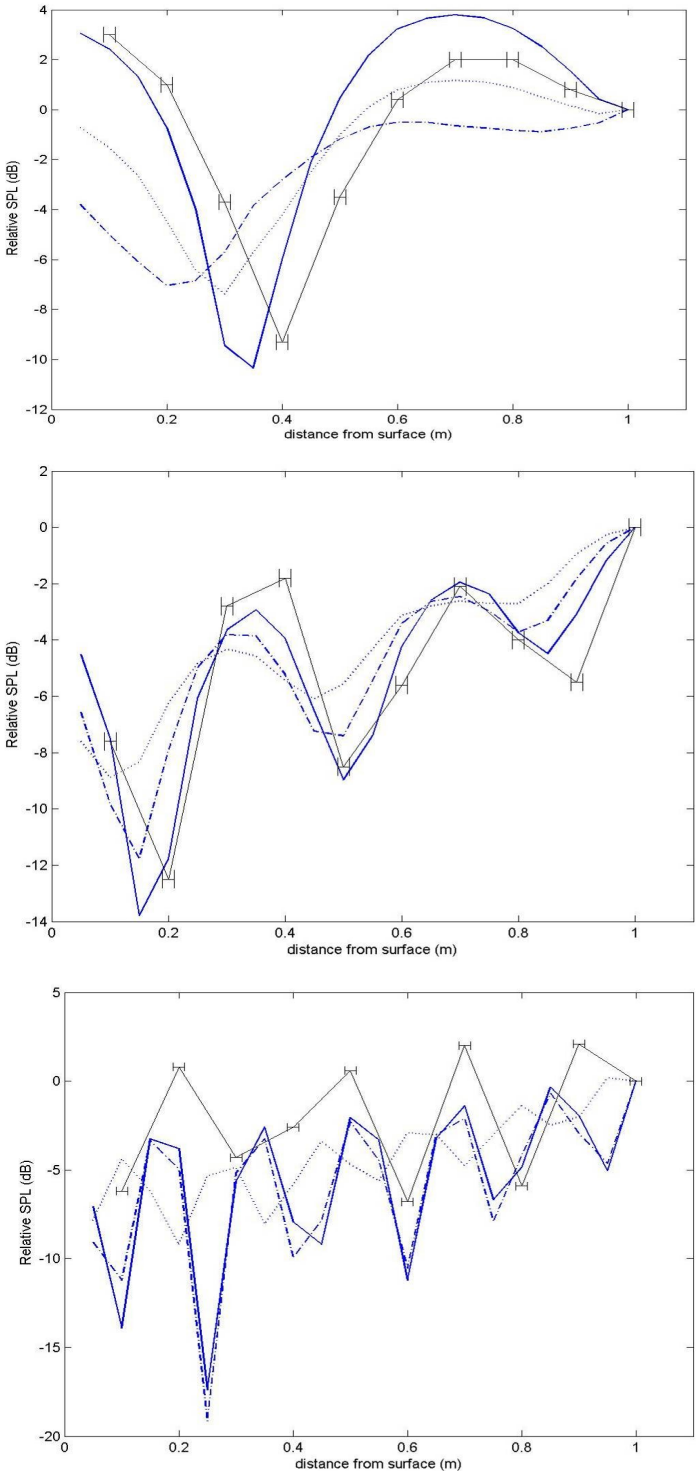

Figure 6.12: SPLs between a surface of carpet and a source at 250 Hz (top), 500 Hz (middle), and 1000 Hz (bottom) (|-| = measured, —— = predicted, real RC, ••• = predicted, impedance tube RC, - - - = predicted, SDM RC).

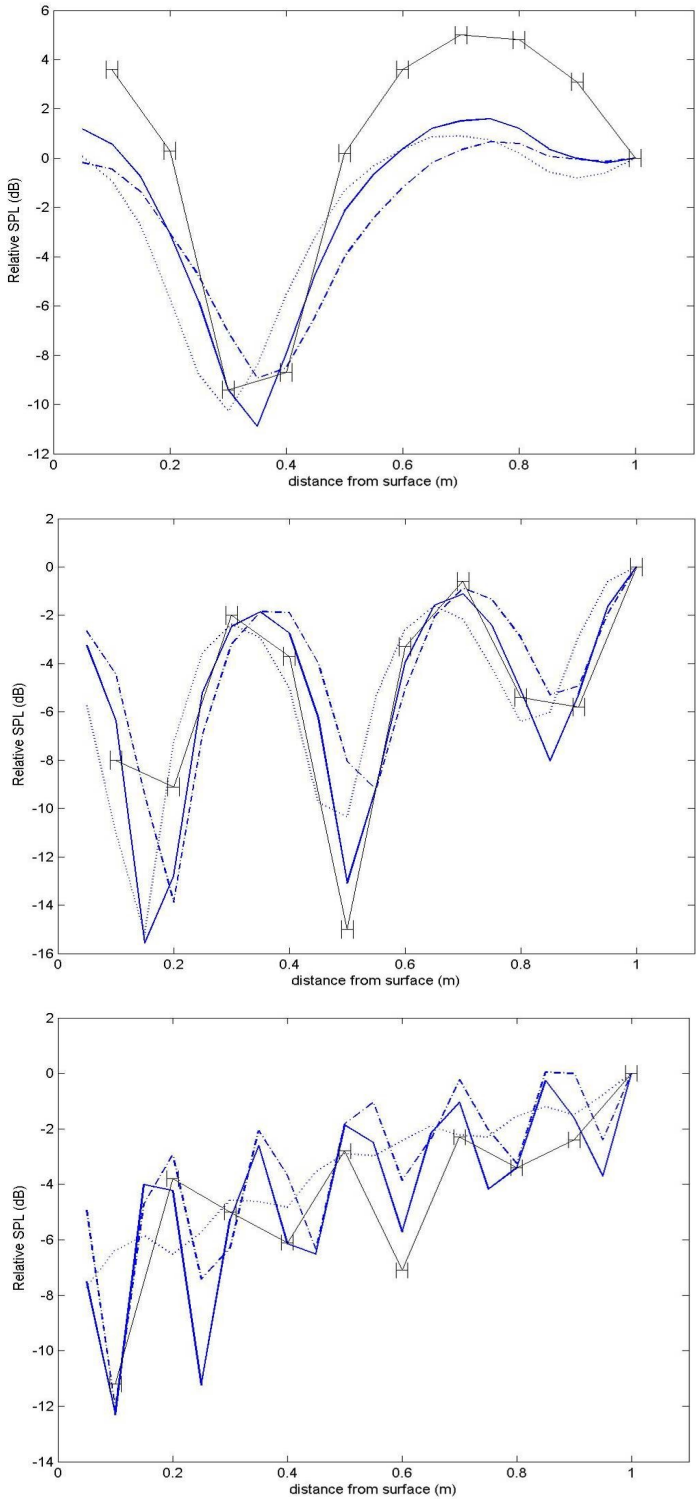

Figure 6.13: SPLs between a surface of ceiling tile and a source, at 250 Hz (top), 500 Hz (middle) and 1000 Hz (bottom) (|-| = measured, —— = predicted, real RC, ••• = predicted, impedance tube RC, - - - = predicted, SDM .RC)

Chapter 6

For further investigation into the accuracy of the prediction model, and of the two methods for determining a surface's reflection coefficients, the same array of microphone positions was used to measure the SPL at ten receiver locations, spaced 10 cm apart, using a source that was producing sound waves with an oblique angle of incidence of 46^0 (where normal incidence is 90^0). A sketch of the experimental setup is shown in Fig. 6.14.

Test surfaces were once again plywood, drywall, acoustical ceiling tile, and carpet. The measured and predicted sound-pressure levels are shown in Figs. 6.15 to 6.18.

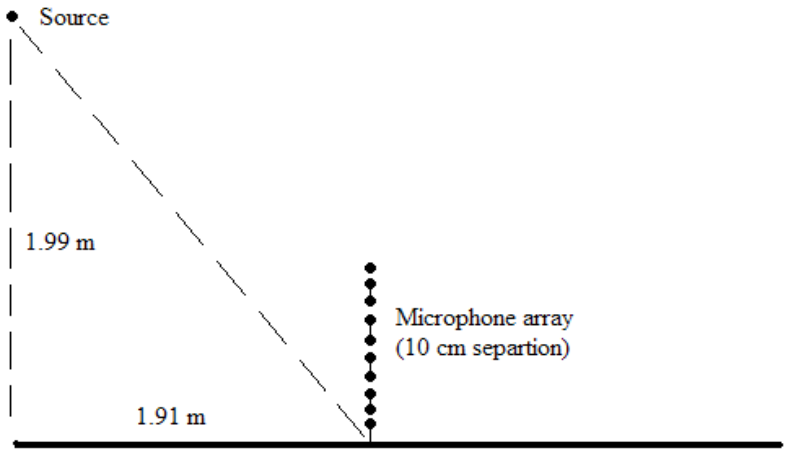

Figure 6.14: Schematic of experimental setup.

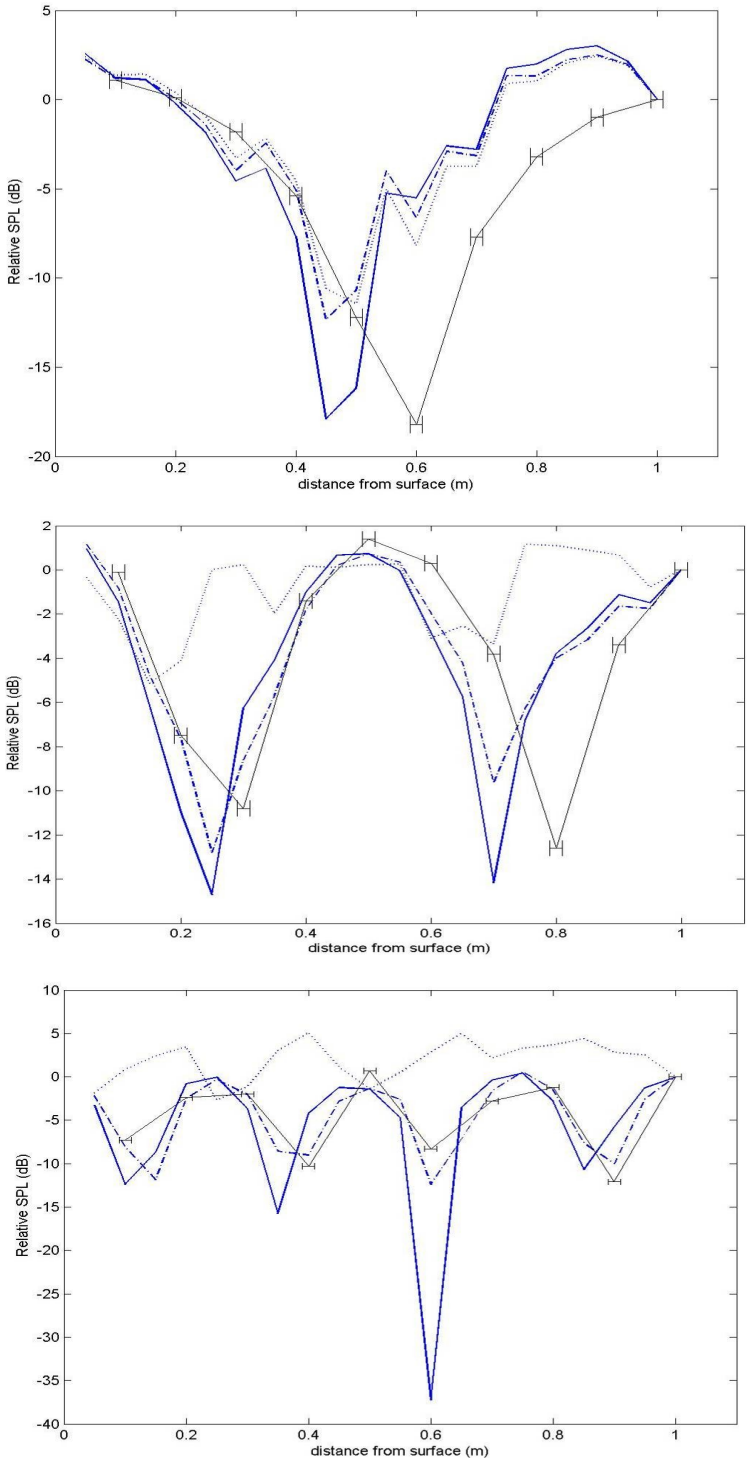

Figure 6.15: SPLs between a surface of plywood and a source with angle of incidence = 46^0, at 250 Hz (top), 500 Hz (middle), and 1000 Hz (bottom) (|-| = measured, —— = predicted, real RC, ••• = predicted, impedance tube RC, - - - = predicted, SDM RC).

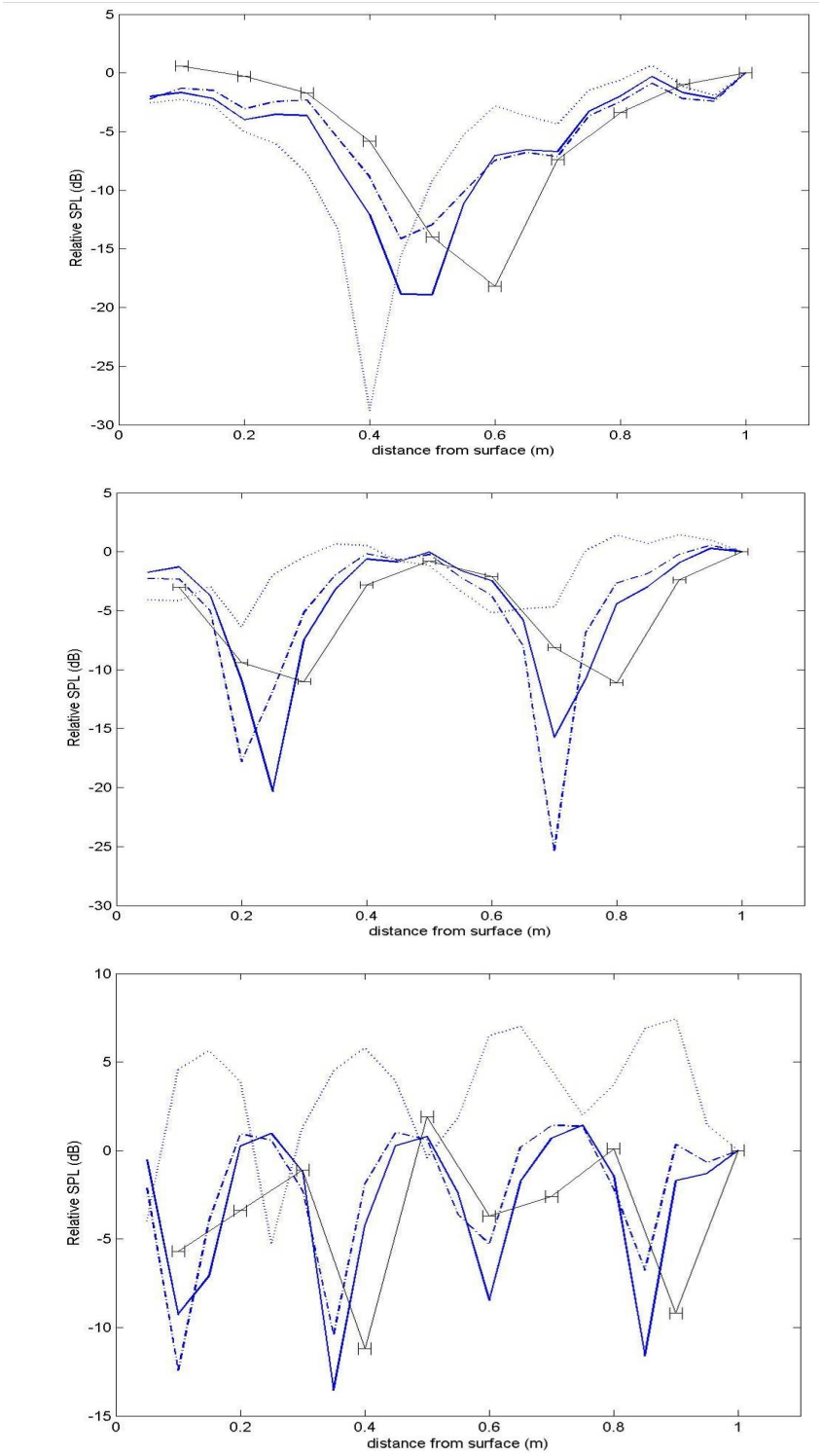

Figure 6.16: SPLs between a surface of drywall and a source with angle of incidence = 46^0, at 250 Hz (top), 500 Hz (middle), and 1000 Hz (bottom) (|-| = measured, —— = predicted, real RC, ••• = predicted, impedance tube RC, - - - = predicted, SDM RC).

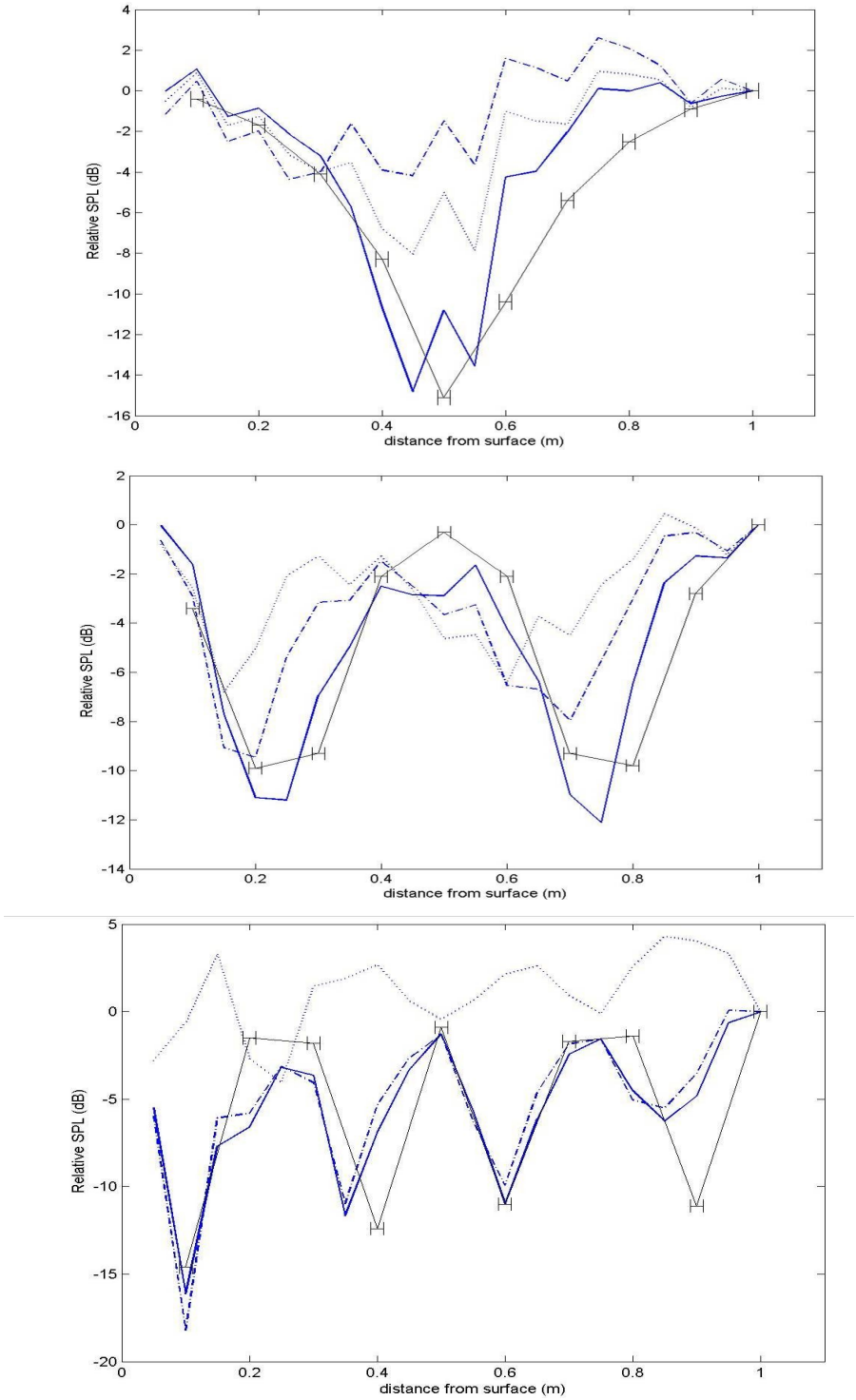

Figure 6.17: SPLs between a surface of carpet and a source with angle of incidence = 46^0, at 250 Hz (top), 500 Hz (middle), and 1000 Hz (bottom) (|-| = measured, ——— = predicted, real RC, ••• = predicted, impedance tube RC, - - - = predicted, SDM RC).

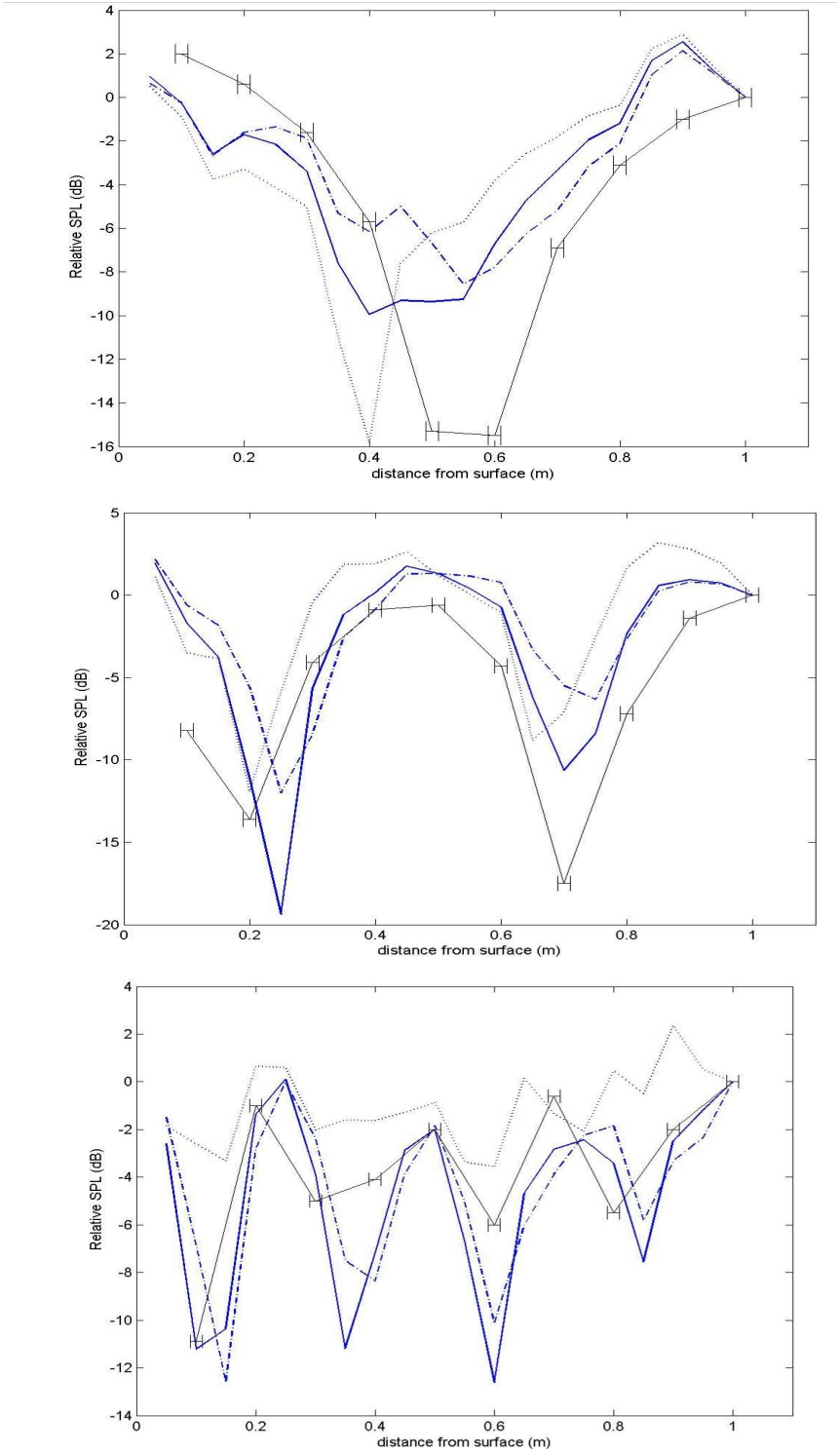

Figure 6.18: SPLs between a surface of ceiling tile and a source with angle of incidence = 46^0, at 250 Hz (top), 500 Hz (middle) and 1000 Hz (bottom) (|-| = measured, —— = predicted, real RC, ••• = predicted, impedance tube RC, - - - = predicted, SDM RC).

Obvious in the above comparisons and predictions is the apparently lower accuracy of the impedance-tube method for finding the complex reflection coefficients of materials. In fact, the complex RCs calculated using the impedance tube were incorrect. This statement can be made since the levels predicted using the RCs defined by this method rarely followed the measured trends. That is to say, the predicted sound-pressure levels contained nodes and antinodes in the vicinity of those measured in six cases, while the levels predicted using the spherical-decoupling method were similar much more often (in nineteen cases). However, it does appear that the impedance tube accurately measures the magnitude of the RC, since predictions using these values are most similar to measured values. In the above predictions, the complex RCs, found using the spherical-decoupling method, were the closest, or equally as close, to the measured values in fifteen out of twenty-four cases. This was not the case for predicted SPLs found using the impedance tube.

6.3 3D intensity above a reflecting plane

After taking sound-pressure measurements above a single plane in the anechoic chamber, it was of interest to measure the 3D intensity at locations above each surface for comparison with predicted intensity levels, in order to achieve the research objectives. Intensity levels were measured in the anechoic chamber in three orthogonal directions, at three heights, over single reflecting surfaces of carpet, drywall, and plywood. A source was located approximately 2 m above the reflecting surface. Figure 6.19 details the experimental setup.

The first surface measured was ½ inch plywood; the source was suspended 2.02 m above the plane, measurement locations were offset 32 cm from the vertical to the source, at heights of 10, 21, and 40 cm. Figs. 6.20 to 6.22 are 2D plots of the predicted versus measured intensity-vector directions in the x-z plane as defined in Figure 6.19.

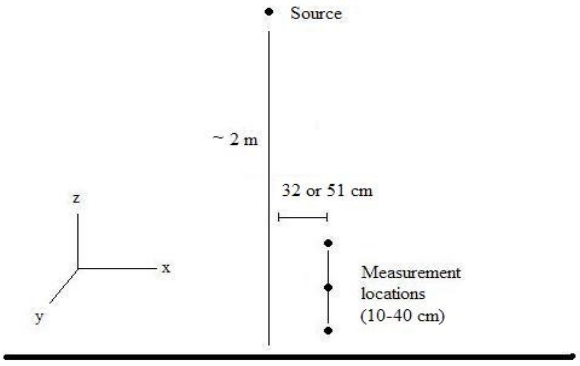

Figure 6.19: Experimental setup for measuring 3D intensity over a single reflecting surface.

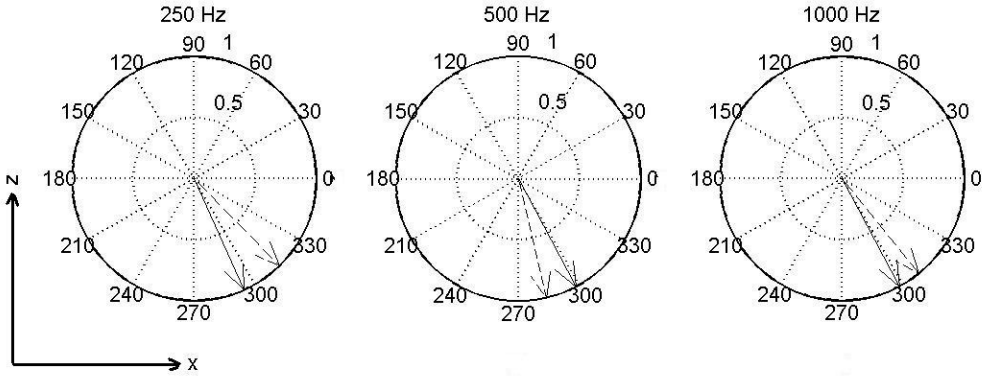

Figure 6.20: Sound-intensity direction in the x-z plane 10 cm above plywood, at 250, 500, and 1000 Hz (- = predicted, -- = measured).

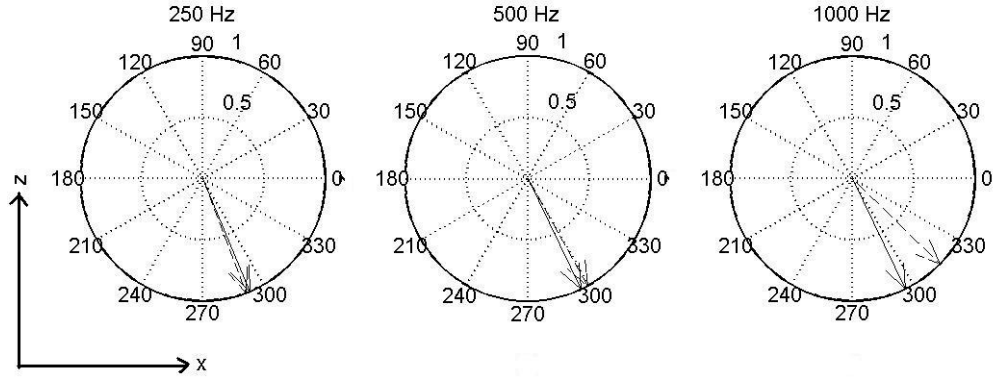

Figure 6.21: Sound-intensity direction in the x-z plane 21 cm above plywood, at 250, 500, and 1000 Hz (- = predicted, -- = measured).

The same comparisons, this time for a surface of carpet, at measurement heights of 11, 22, 40 cm are shown in Figs. 6.23 to 6.25.

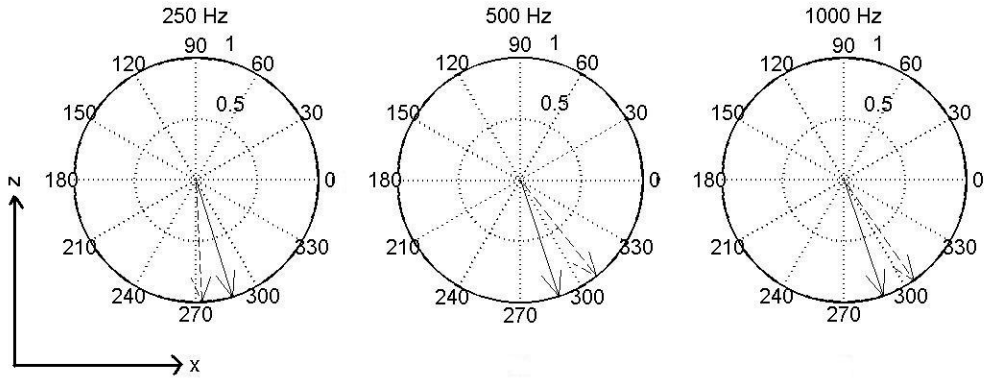

Figure 6.22: Sound intensity-direction in the x-z plane 40 cm above plywood, at 250, 500, and 1000 Hz (- = predicted, -- = measured).

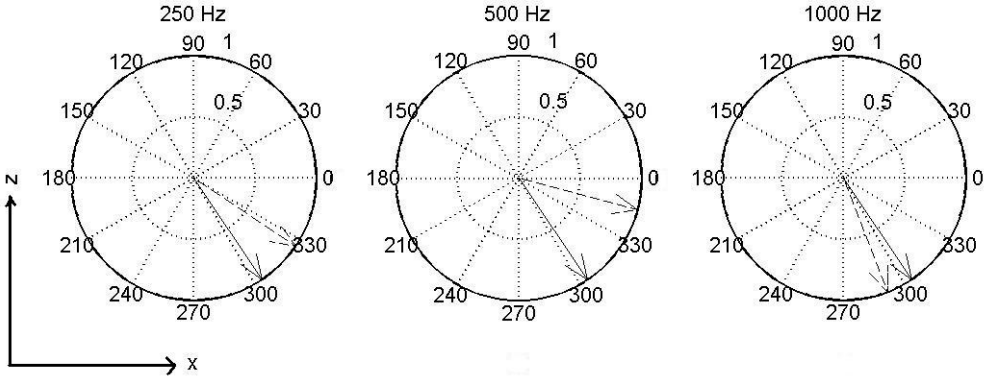

Figure 6.23: Sound-intensity direction in the x-z plane 11 cm above carpet, at 250, 500, and 1000 Hz (- = predicted, -- = measured).

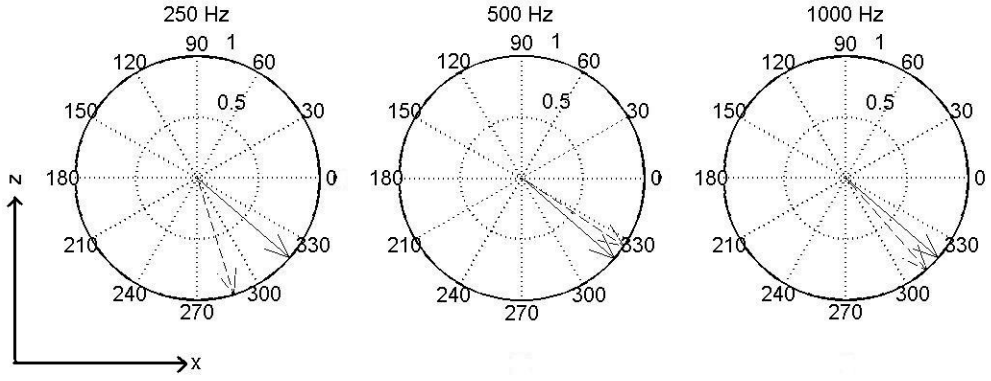

Figure 6.24: Sound-intensity direction in the x-z plane 22 cm above carpet, at 250, 500, and 1000 Hz (- = predicted, -- = measured).

Finally, for a surface of drywall, with a measurement offset of 51 cm, at heights of 13, 23, 36 cm, the results are shown in Figs. 6.26 to 6.28.

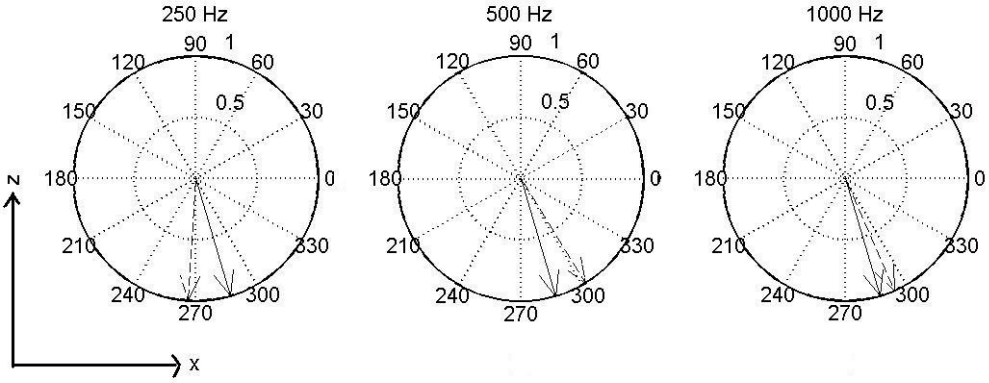

Figure 6.25: Sound-intensity direction in the x-z plane 40 cm above carpet, at 250, 500, and 1000 Hz (- = predicted, -- = measured).

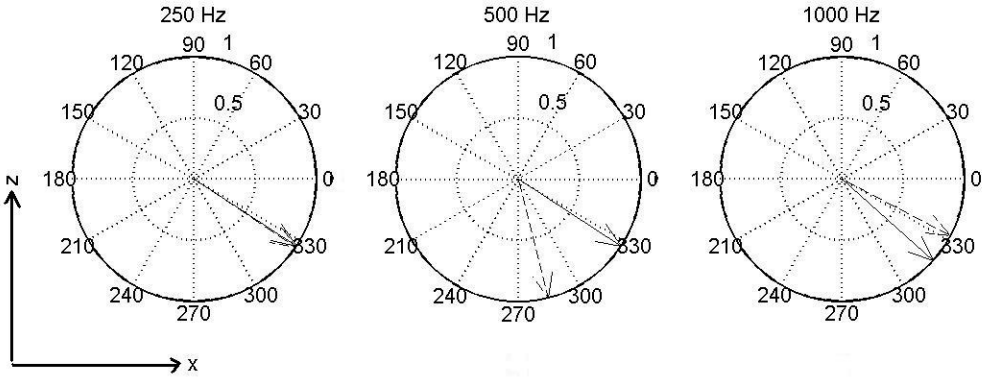

Figure 6.26: Sound-intensity direction in the x-z plane 13 cm above drywall, at 250, 500, and 1000 Hz (- = predicted, -- = measured).

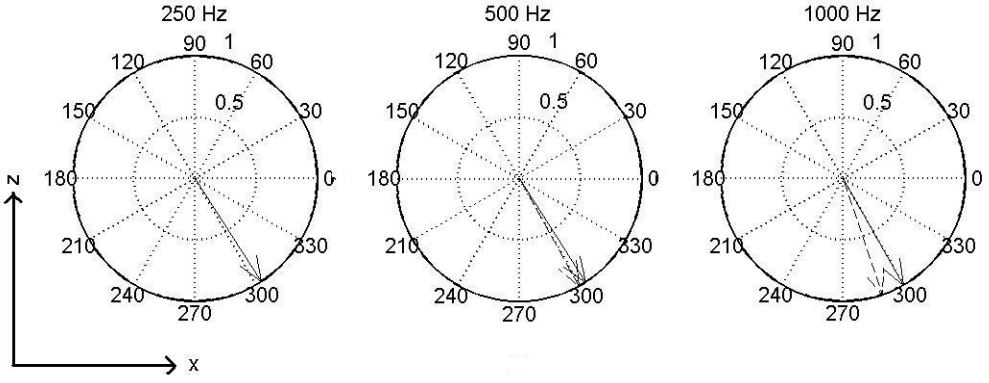

Figure 6.27: Sound-intensity direction in the x-z plane 23 cm above drywall, at 250, 500, and 1000 Hz (- = predicted, -- = measured).

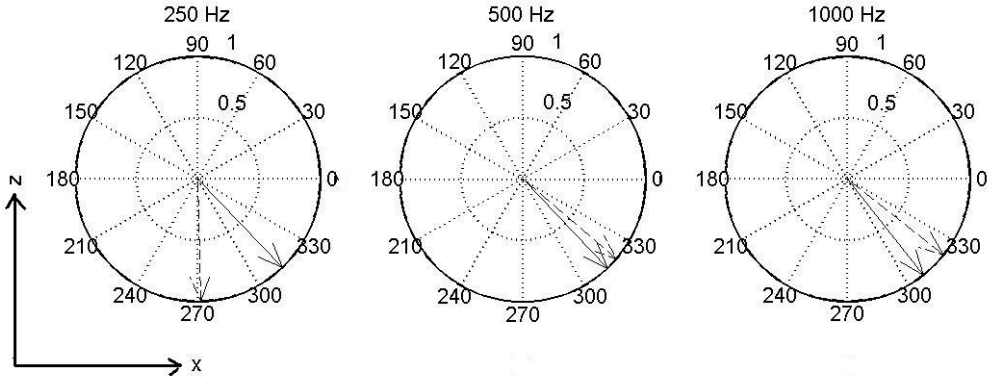

Figure 6.28: Sound-intensity direction in the x-z plane 36 cm above drywall, at 250, 500, and 1000 Hz (- = predicted, -- = measured).

Considering the fact that, of twenty-seven predictions, only thirteen were in agreement with the measured intensity direction in the x-z plane, these results do not provide evidence of accurate prediction. However, the number of accurate predictions is greatest for the drywall reflecting surface, and least accurate for plywood. This may be attributed, at least in part, to incorrectly measured complex reflection coefficients for those surfaces with poor results, a statement based on the irregularities in their reflection coefficients, especially at lower frequencies. Another trend in the comparisons is the fact that the accuracy of those predictions increases with frequency. The greatest number of accurate predictions, six out of nine cases, occurs at 1000 Hz, with the next best being four cases at 500 Hz, followed finally by three at 250 Hz. The reasons for this could include instrumentation accuracy that increases with frequency due to intensity-probe spacer-size effects. However, it is more likely to be due to the use of inaccurately measured reflection coefficients at low frequencies. One final tendency to note is that the predicted values were most often similar to those measured at receiver heights that were neither especially close to the reflecting surface, nor to the sound source. Seven of nine possible predictions were similar to those measured at the middle measurement position. This may be due to the fact that, for measurement locations near either the source or the reflecting plane, the plane-wave assumption made in the prediction model is less valid, as sound waves spread spherically from most sources. Near-field and edge diffraction effects could also cause discrepancies between predicted and measured values. Near-

field effects would become increasingly noticeable the nearer the intensity probe was to either the source or the reflecting surface, while edge-diffraction effects increase with distance from the surface. The reflection coefficients used in prediction were measured at heights above the surfaces different from the heights of the intensity-probe during sound-intensity measurement. Near-field and edge-diffraction effects would affect measurements differently depending on their heights. For higher prediction accuracy and better agreement, the complex reflection coefficients would have to be measured at the same heights as those used for intensity measurement. This would require larger sample surface areas, in order to prevent non-negligible edge effects, and surfaces that would not fit within the anechoic chamber used in this research.

6.4 Sound-pressure level in a scale-model room

After measuring sound-pressure and sound-intensity levels in an anechoic chamber, it was decided that further investigation into the accuracy of ORAYCUB was necessary. Comparing results measured and predicted for actual rooms, with multiple reflecting surfaces, was the next step in experimental comparison. The first room measured was a ¼-scale-model room with actual dimensions of 1.88 x 1.91 x 0.91 m^3 (full-scale dimensions of 7.52 x 7.64 x 3.64 mFS^3 – FS = full-scale equivalent dimension). Predicted sound-pressure levels were compared to those measured with a 4 inch loudspeaker in a corner, on a plane covering half of the room's floor plan, with a grid size of 20 cm x 20 cm, as shown in Fig. 6.29.

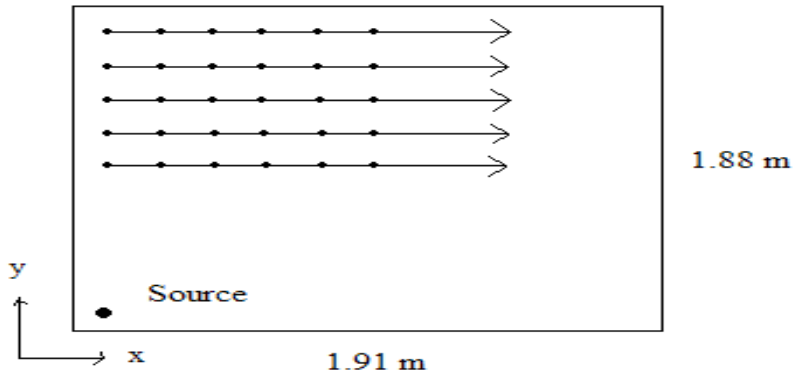

Figure 6.29: Floor plan of scale-model room including source and measurement locations.

Chapter 6

Pressure levels were measured as 10 s averaged LEQ. The four walls and the ceiling of the scale-model room consisted of ¼" wood panels, while the floor was polished concrete. Measurements were made at three frequencies, with two microphone heights of 31 cm and 69 cm. Figs. 6.30 to 6.33 show the results, including the six measured and predicted contour plots, as well as six cross-sectional graphs of the sound field for each measurement, showing both predicted and measured levels. All cross-sectional values are normalized to the mean SPL, since the sound-source power output was not calibrated.

It is difficult to discern from the contour plots of the sound field how well the predicted values approximate the measured sound field. Nodes and antinodes are obvious in both sets of data, something that would be completely absent when using the original RAYCUB program, although their locations do not often match. There are a number of reasons for the differences in the location and amplitudes of the nodes in the sound field, including the previously mentioned finite receiver-volume effect, and the subsequent averaging that occurs over every receiver location. Also important to note is the fact that the measured sound field was not produced using a perfect point source, as in the prediction model; instead a baffled 4" (16" full-scale dimension) loudspeaker was used. This, along with the fact that the scale model has poorly sealed surfaces, would likely reduce the accuracy of prediction of the sound field. For this reason, sound-fields were next measured in a full-size, tightly-sealed room for comparison with prediction.

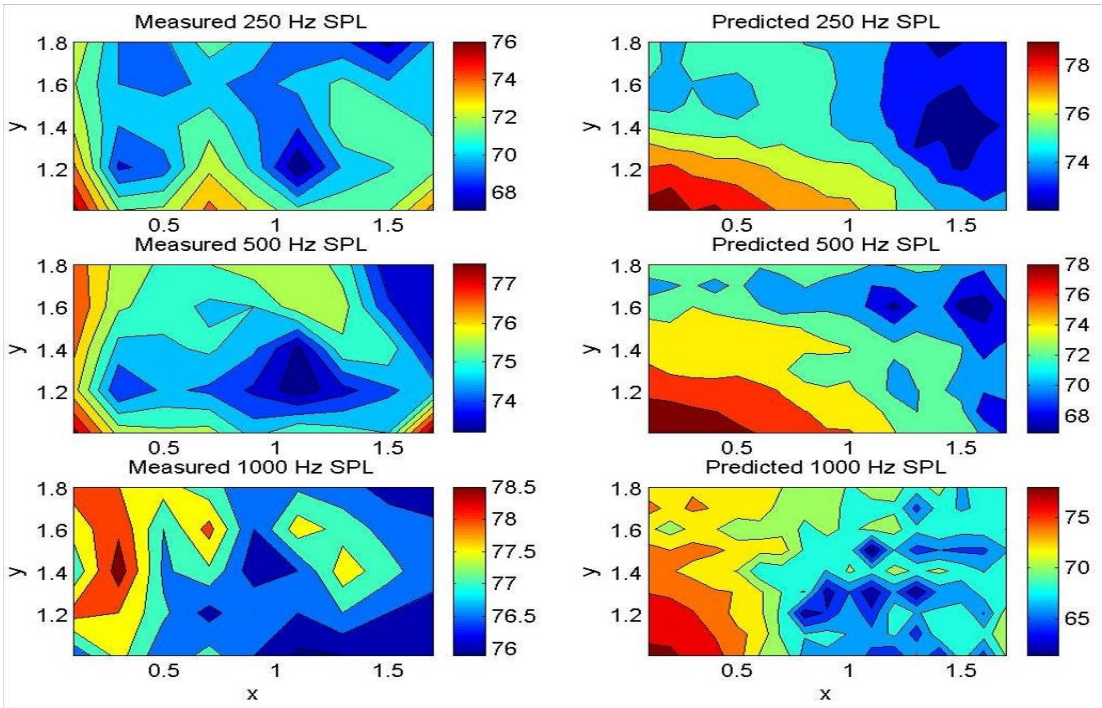

Figure 6.30: Contour plots of the measured (left) and predicted (right) sound-pressure levels at a receiver height of 31 cm in the scale-model room at 250, 500, and 1000 Hz.

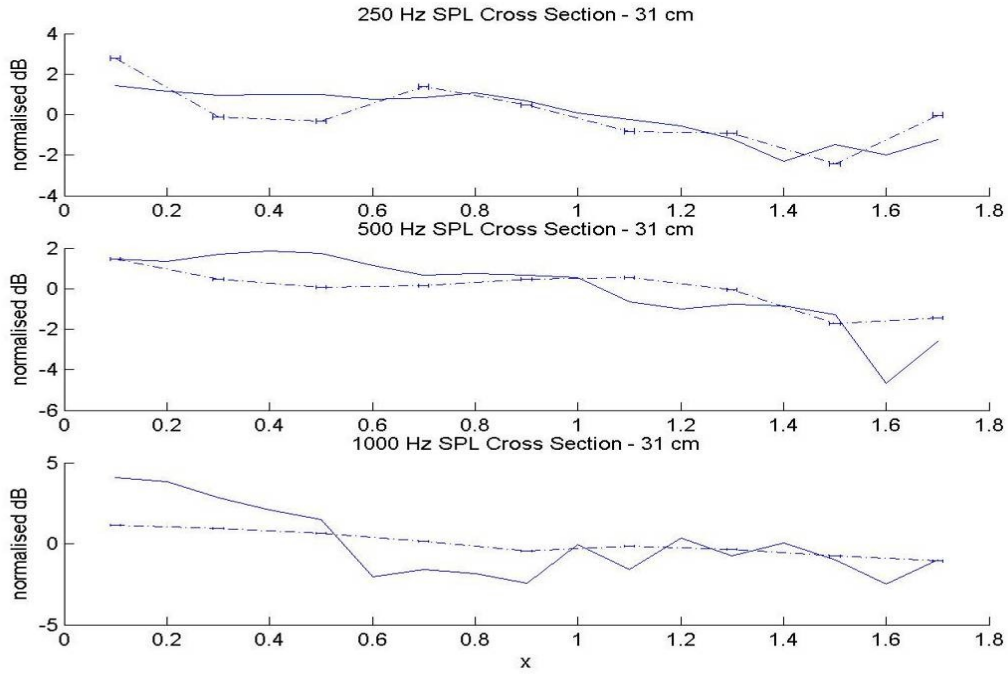

Figure 6.31: Cross-sectional variation of sound-pressure levels at y =1.38 m, measured at a height of 31 cm in the scale model (▬ predicted, |-| measured)

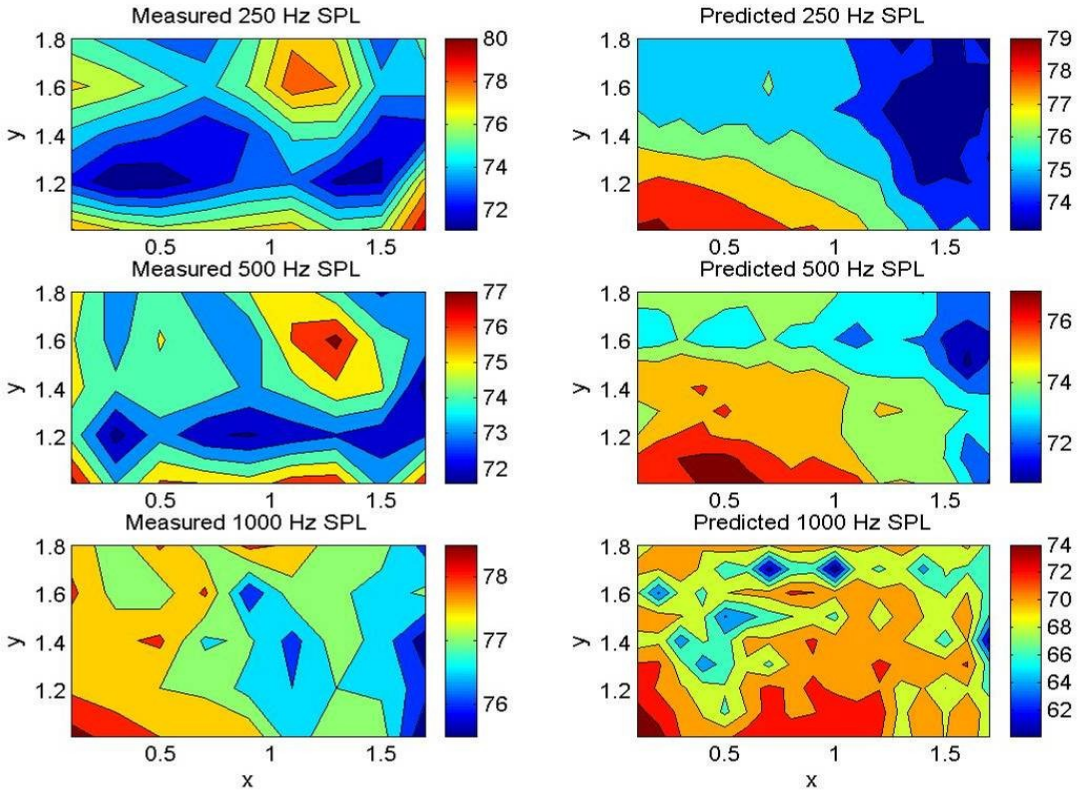

Figure 6.32: Contour plots of the measured (left) and predicted (right) sound-pressure levels at a receiver height of 69 cm in the scale-model room at 250, 500, and 1000 Hz.

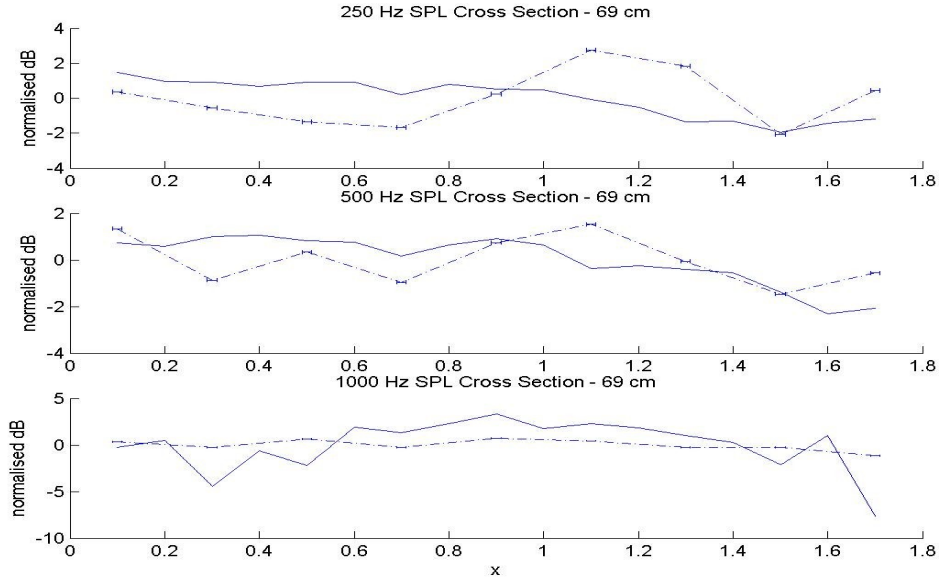

Figure 6.33: Cross-sectional variation of sound-pressure levels at y =1.38 m, measured at a height of 69 cm in the scale model (—— predicted, |-| measured).

The cross-sectional variations of the predicted and measured sound fields (Figs. 6.31 and 6.33) provide information that is easier to compare, and these results agree relatively well. In all cross-sectional graphs, the amplitudes of predicted nodes and antinodes do not vary more than 5 dB from those measured, with the usual value being less than 2 dB. General trends of the location of these maxima and minima in SPL agree. Results at 1000 Hz agree less well since, at this frequency, the measurement resolution is insufficient to accurately portray the modal response of the scale-model room.

6.5 Sound-pressure levels in a full-scale room

The final environment for comparison of prediction with experiment was a full-size room with dimensions 5.39 x 2.4 x 2.76 m^3. One wall consisted of double-paned glass, while the other three were drywall. The ceiling was composed of acoustical ceiling tile and flush-mounted fluorescent lights, while the floor was linoleum tile on concrete. Sound-pressure levels were predicted and measured on three receiver arrays, each a section of one of the axes of the room, denoted here as Arrays X,Y, and Z as shown in Figure 6.34. A 40 cm diameter omni-directional loud speaker array was placed in a corner with its centre at coordinates (0.22, 2.18, 0.28); SPLs were measured at frequencies of 250 Hz, 500 Hz, and 1000 Hz. Measurements were made every 10 cm, using 10 s Leq averaging, with no-one present in the room.

The first cross-section (Array X) of receiver locations that was measured was in the x direction from x = 0.1 to 5.3 m, while holding y and z coordinates constant at 1.26 m and 0.835 m, respectively. Fig. 6.35 shows the results for both measured and predicted sound-pressure levels, at the three frequencies. The cross-section in the y direction (Array Y) was measured with y ranging from 0.1 m to 2.3 m, with constant x and z values of 2.34 m and 0.625 m. Fig. 6.36 shows the resulting measured and predicted SPLs. The final cross-section, in Fig. 6.37 (Array Z) was measured from the floor to ceiling at z coordinates ranging from 0.1 m to 2.5 m. The x and y coordinates were fixed at (2.75, 0.94) m.

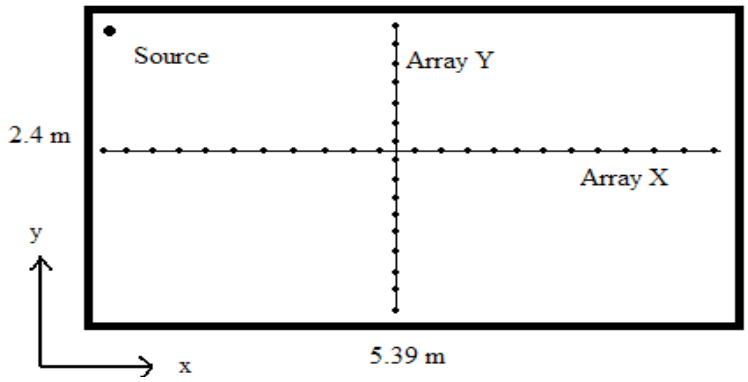

Figure 6.34: Floor plan of the full-scale room, showing room dimensions, as well as source and measurement locations.

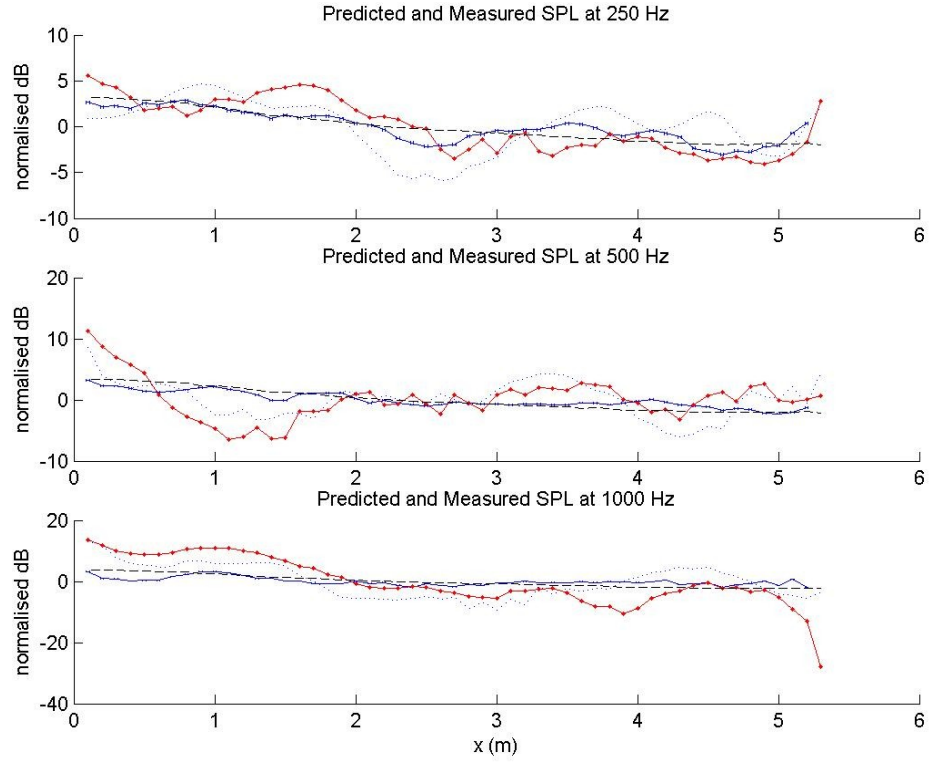

Figure 6.35: Predicted and measured SPLs in a room along Array X, at 250 Hz (top), 500 Hz (centre), and 1000 Hz (bottom)

(|-| measured, - - - RAYCUB, ••• ORAYCUB, —●— ORAYCUB DC=0.5)

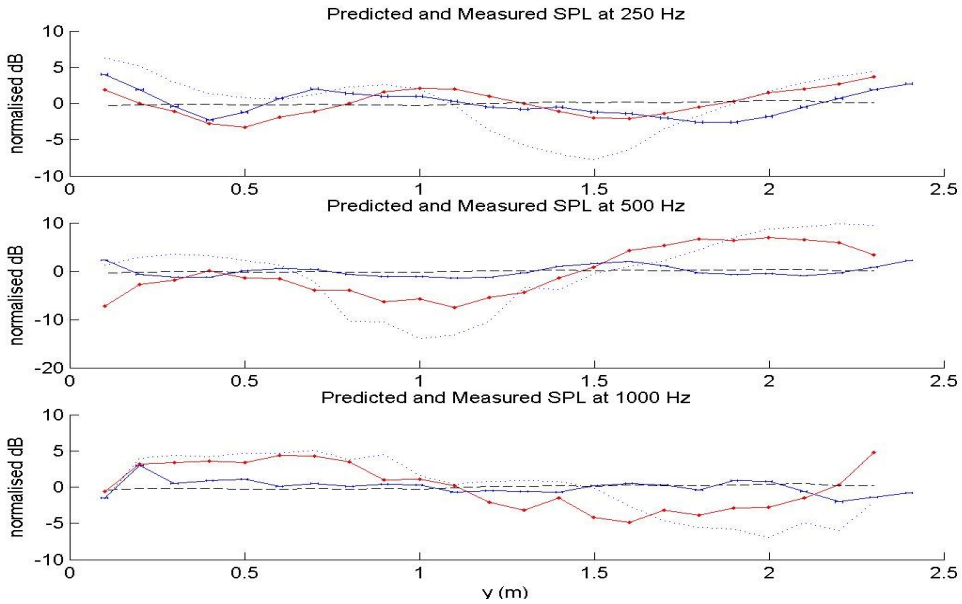

.Figure 6.36: Predicted and measured SPLs in a room along Array Y, at 250 Hz (top), 500 Hz (centre), and 1000 Hz (bottom)

(|-| measured, - - - RAYCUB, ••• ORAYCUB, ORAYCUB DC=0.5).

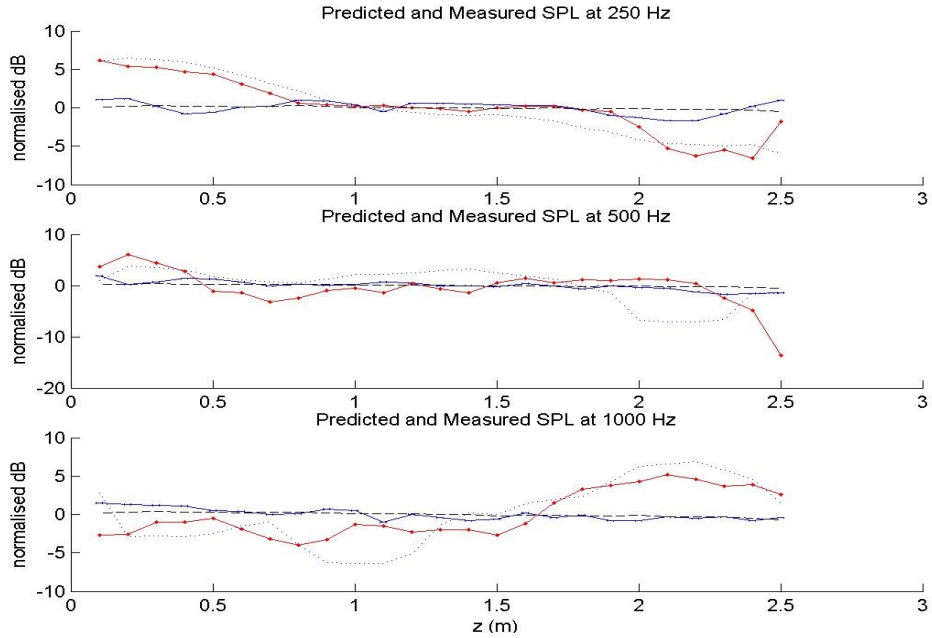

Figure 6.37: Predicted and measured SPLs in a room along Array Z, at 250 Hz (top), 500 Hz (centre), and 1000 Hz (bottom)

(|-| measured, - - - RAYCUB, ••• ORAYCUB,. ORAYCUB DC=0.5).

The accuracy of the predicted SPLs in the full-scale room using the new model appears to be frequency dependent. At lower frequencies, the modal behaviour of the room is well predicted, with the sound-pressure levels varying "in-tune" with the levels measured. That is to say, general fluctuations or trends in the sound pressure-levels are modeled. At higher frequencies, the improved model predicts modal behaviour that is not present in the measured sound field. In one regard, the new prediction model is less accurate than RAYCUB since the SPLs predicted using ORAYCUB, compared to those predicted using RAYCUB, vary to a greater extent from measured SPLs. In another regard, it can also be stated that the new program is a more accurate prediction model than the original program at lower frequencies, since modal behaviour is modeled, whereas it is absent in the original predicted levels. At higher frequencies, the new model appears to be less accurate, since modal behaviour that is not measured is predicted. The original program, unable to account for phase effects, is absent of this phenomena. Further comparison, with a better controlled full-scale room with more regular dimensions and well known complex reflection coefficients, is necessary to determine over what frequency range the new model is an improvement.

Another phenomenon in Figs. 6.35-6.37 that is interesting to note is the effect that different diffusion coefficients have on the ORAYCUB predicted SPLs. Although the complex RCs used in prediction were found using the SDM, which assumes specular reflection, SPLs were predicted using a DC of 0.5 for all surfaces as well, in order to demonstrate the effect of the DC on prediction. This demonstrates a benefit of the new prediction model, ORAYCUB can be used to inversely determine boundary conditions such as DCs and RCs by finding the best fitting parameters. This is true for ORAYCUB and not RAYCUB because RAYCUB does not agree with the validation attempts outlined in Section 5.

6.6 Sound intensity in a full-scale room

Using the same full-size room of dimensions 5.39 m x 2.4 m x 2.76 m, one final comparison with measurement was made. That was to compare the predicted three-

dimensional intensity-vector directions at two receiver locations. In the room, these points were defined by the intersection of two lines, one a plumb line suspended from the ceiling, the other a line intersecting the room in the Y plane. The three components of the intensity vector were measured separately using a Bruel and Kjaer Type 3545 intensity probe with a 50-mm microphone spacer, and a Norsonics Type 830 Real Time Analyser. The three orthogonal components were summed vectorally. Measurements were made at three frequencies of 250 Hz, 500 Hz, and 1000 Hz with the omni-directional source located in the corner at (0.32, 2.13, 0.28). Results for the first measurement, located at (1.31, 0.37, 0.85), are shown in Figs. 6.38 to 6.40.

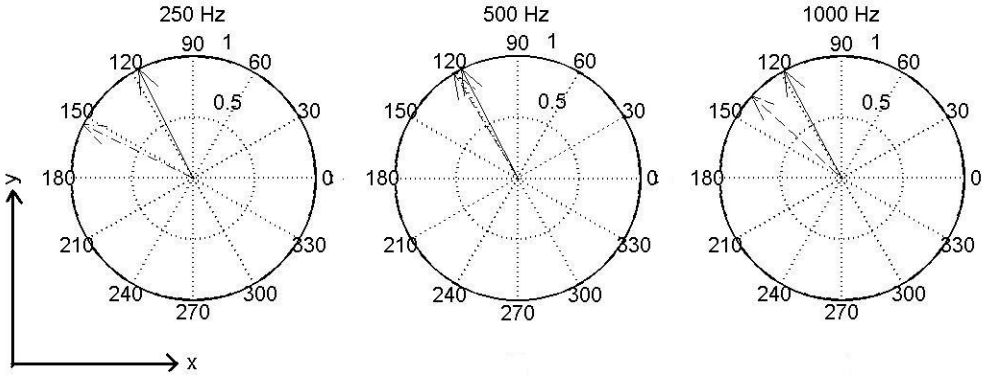

Figure 6.38: Measured and predicted compass plots, in the XY plane, of the sound-intensity direction for location 1 in the full-scale room (- predicted, -- measured).

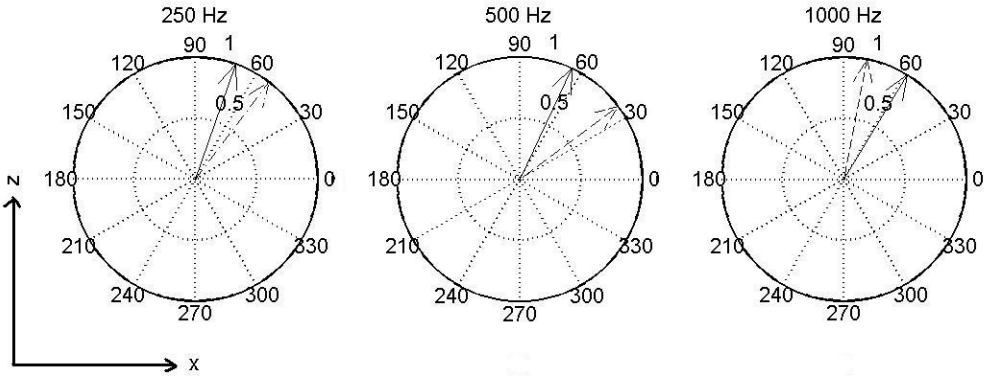

Figure 6.39: Measured and predicted compass plots, in the XZ plane, of the sound-intensity direction for location 1 in the full-scale room (- predicted, -- measured).

The second measurement location was (2.79, 1.09, 0.85); Figs. 6.41 to 6.43 show those results.

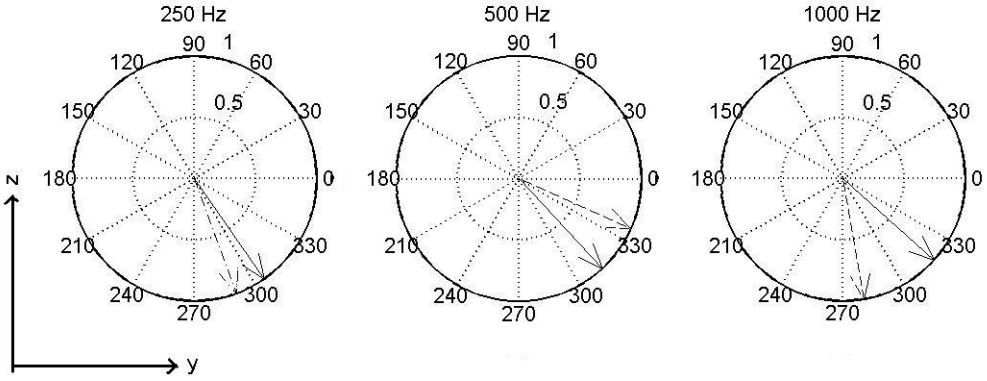

Figure 6.40: Measured and predicted compass plots, in the YZ plane, of the sound-intensity direction for location 1 in the full-scale room (- predicted, -- measured).

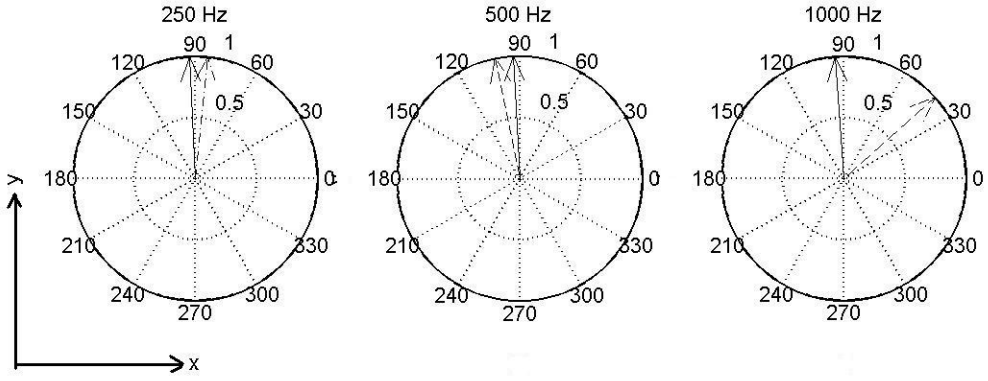

Figure 6.41: Measured and predicted compass plots, in the XY plane, of the sound-intensity direction for location 2 in the full-scale room (- predicted, -- measured).

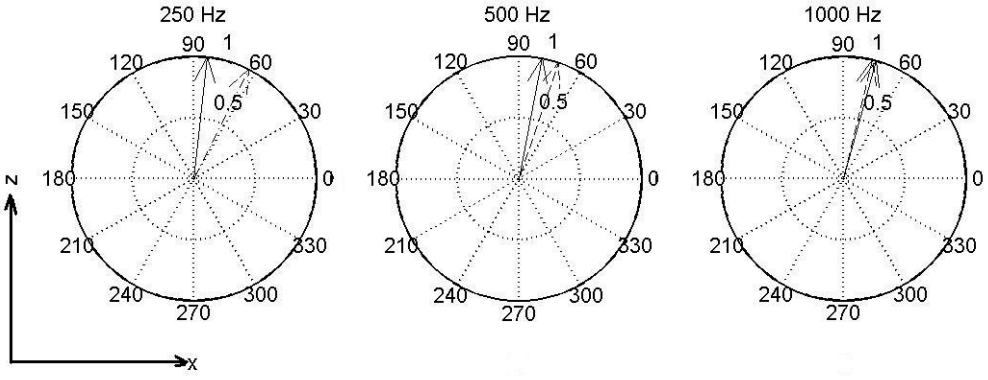

Figure 6.42: Measured and predicted compass plots, in the XZ plane, of the sound-intensity direction for location 2 in the full-scale room (- predicted, -- measured).

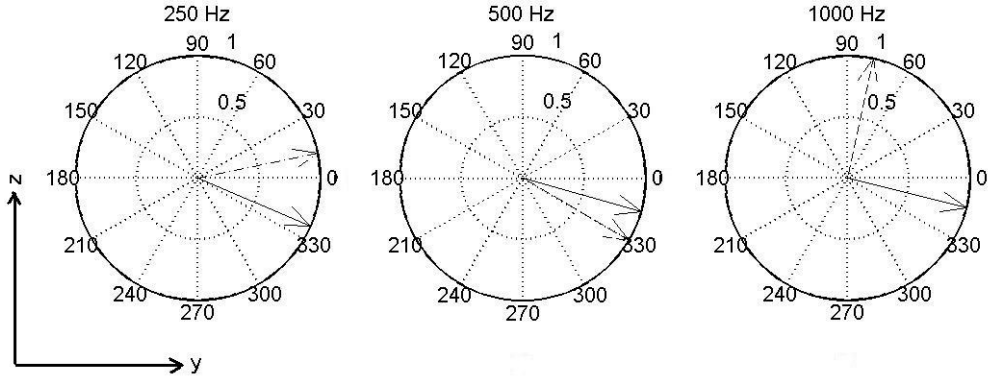

Figure 6.43: Measured and predicted compass plots, in the YZ plane, of the sound-intensity direction for location 2 in the full-scale room (- predicted, -- measured).

Every predicted intensity direction is within 90^0 of the measured direction for all 18 compass plots above, with most very much closer. Twelve of the eighteen predicted intensities are very close (within 25^0) to the measured direction; seven of these are within 15^0. These results are more impressive than they seem at first. Considering the fact that glass-plane RCs were approximated, that the entire room contained a non-negligible, non-modeled, wooden hand rail, and that two doors and one elevator entrance were present but not modeled, predicting a real-room intensity vector to within 25^0 two thirds of the time is good.

Chapter 7

Error sources

The results presented in this work are affected by numerous sources of error. These errors include differences between predicted and measured sound-pressure levels, intensity directions, and possibly the locations to which they are assigned. Errors sources can be divided into two groups: those that affect measured values, and those that affect prediction accuracy.

7.1 Prediction errors

One source of error in the prediction algorithm, present in all cases, is the finite receiver volume. This has already been mentioned in Section 5.2 but, in summary, the program algorithm requires the user to define the size of the cubic receiver used in the prediction. This may lead to inconsistencies between predicted and measured values, since measured values are typically found using a ½ inch microphone; whereas sound-pressure levels predicted, and assigned to one specific point, in fact include the total pressure contributions of all rays within the receiver volume surrounding the measurement point. This has the greatest effect when the receiver is located at a node in the sound field. A microphone placed at this location averages the SPL across its relatively small area and measures a low SPL. ORAYCUB, instead of averaging the SPL over a small surface area, averages the SPL over the entire receiver volume, including areas of less than perfect destructive interference. This results in nodes and anti nodes of lower amplitude. These effects can be reduced by decreasing the size of the receiver volume, but at a runtime cost that is two-fold; by reducing the receiver volume, more receivers are necessary for the prediction of a sound field, thereby increasing the run time and memory requirements of the program, and also the reduced volume of such a receiver requires a much greater number of rays to be tracked to obtain high accuracy by ensuring that a sufficient number cross the receiver cell. As is the case with most prediction models, there is always a trade off between accuracy and computation cost.

Another error, present in the original code for RAYCUB and still present in ORAYCUB, is the fact that, should a receiver cell contain a sound source, unrealistically high sound-pressure levels are predicted. The reason for this is that the original implementation for calculating an incident ray's pressure contribution to a receiver cell is calculated using the distance the ray travels through the receiver cell, by considering the points on the cell surfaces where the ray enters and exits. In the case where the source is in the cell, a ray does not pass through, but simply exits a cell, and this algorithm breaks down. Users of this program should be aware of this fact and either ensure that a receiver cell does not contain a source or, if such a case is not preventable, the user should ignore any values predicted for such a cell.

One final error or, more accurately, one assumption made, is that sound sources emit rays with a uniformly random direction. That is to say, the modeled sources are all omni-directional. Sources used in this research were not always omni-directional.

7.2 Measurement Errors

It should first be stated that all data measured and reported within this work was acquired with the use of instruments of a high standard. Instrumentation error is inherently therefore very limited, if not negligible. Sound level meters and intensity meters were calibrated before use, resulting in levels that are accurate within 1 dB.

One source of error that cannot be neglected is the uncertainty in measurement locations within the anechoic chamber. This is due to the fact that the floor of the anechoic chamber is a suspended wire mesh. This mesh is very taught, but nevertheless sags under the weight of an experimental setup and the experimenter. Therefore, locations of objects, including reflecting surfaces and microphones, in contact with the floor could be inaccurate by up to 1 cm. The effect of such a change in microphone or sound-source location is greatest at higher frequencies.

Another possible source of error in this work is that the three components of the 3D intensity levels may not have been perfectly orthogonal, since a two microphone probe was used. It was necessary to make three separate measurements at each location, defined by the intersection of two orthogonal reference lines. The effect of the intensity

probe being off axis was great, for when the probed moved during measurement, changes in the intensity level were obvious. Errors between measurements were not possible to detect since it was only possible to recognize changes in levels during a single measurement.

In this study baffled loudspeakers of sizes ranging from 4 to 8 inches were used. Such a sound source emits sound waves in a non uniform, directional matter. The directional behaviour of loudspeakers is not modeled in ORAYCUB.

A final and perhaps most important source of error is the difference between the actual location of a sound source, and the point source assumed to model it. It is difficult to model a loudspeaker enclosure with a side length of 12 inches by a point source, since the sound field created by such a source is not the same as that created by a point source placed at the position of the centre of the loudspeaker, directional concerns aside. That is to say, the effective point from which sound energy is radiated may not be its centre, but may be at a point in front of the vibrating cone. A brief study was conducted in order to ascertain the location of this point for the 8 inch loudspeaker enclosure used most often in this study.

Free-field theory for a point source states that the sound pressure in an environment absent of any reflecting surfaces decreases by 6 dB for every doubling of distance. The sound-pressure level SPL(2) was measured in the anechoic chamber 2 m in front of the loudspeaker. The SPL was then measured at distances greater than 2 m, until the reported value was 6 dB lower than the values measured at 2 m. According to free-field theory, this distance is equal to twice the distance separating the effective point-source position and the first receiver position. Therefore the effective point-source position is the same distance from the first measurement location as the distance between the receiver at SPL(2) and the receiver position at which the SPL is 6 dB lower. Fig. 7.1 is a summary of the experimental setup, and Table 7.1 of the results found.

Chapter 7

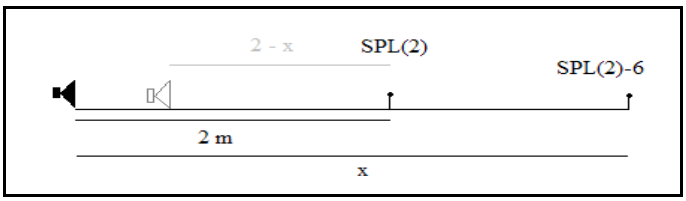

Figure 7.1: Schematic showing locations of source, two microphones, and effective source location.

Table 7.1: Calculating the effective point-source location for an 8" loudspeaker.

frequency (Hz)	SPL(2) (dB)	x (m)	SPL(x) (dB)	difference (dB)	x-d (m)
250	84.9	3.1	79.1	5.8	1.1
250	**84.9**	**3.15**	**78.7**	**6.2**	**1.15**
250	84.9	3.3	78.5	6.4	1.3
500	90.5	3.1	84.7	5.8	1.1
500	**90.5**	**3.15**	**84.4**	**6.1**	**1.15**
500	90.5	3.2	84.3	6.2	1.2
1000	98.3	3.2	93.2	5.1	1.2
1000	98.3	3.3	93.1	5.2	1.3
1000	**98.3**	**3.4**	**92.2**	**6.1**	**1.4**

If SPL(x) = SPL(2) – 6 dB, then the effective source location is actually 2-x metres from the first microphone.

As shown by the bold figures in Table 7.1, the effective point-source location for the 8 inch loudspeaker enclosure used for the majority of the experimental work is never at the centre of the speaker box. In fact, the effective location is greater than half a meter in front of the source, for all frequencies used. This is further compounded by the inconsistency of the calculated location since variances between repetitions of this study were great. In all predictions made in this study, sound-source locations were still assigned the same exact location as the centre of an omni-directional loudspeaker, or the front of the vibrating diaphragm in a standard loudspeaker.

Chapter 8

Conclusions

The objective of this work was to create a room-prediction model which predicted sound-pressure levels to a high degree of accuracy, as well as predicting accurate steady-state and transient-sound-intensity levels.

To obtain the detailed research objectives, an existing ray-tracing model, RAYCUB, was modified in order to account for phase effects and predict sound intensity. The original program was an energy-based model, accurate at high frequencies at which room modal responses are less evident. In order to lower the frequency restrictions for accurate sound-pressure level prediction, the program was modified to track the complex pressure of a ray, instead of its energy. This permitted the complex addition of ray pressures as they were received, where the phase of any given ray was affected by the path length it traveled, and the phase delays imparted by reflection from surfaces with complex, finite impedances. The program was further modified to cumulatively sum the received ray pressures using vector addition in order to predict the sound-intensity level, a measure not only of the total sound-field amplitude, but also of the direction of energy flow. This was implemented such that a total, steady-state intensity was predicted, as well as time-binned transient intensity with a user-defined time resolution.

To ascertain whether modifications were implemented correctly, the new prediction model was validated. The first part of validation included investigating the prediction accuracy and its dependence on user-defined parameters. It was shown that receiver cells with smaller volume require increasingly more emitted rays, therefore increasing computational cost. In an anechoic environment, 10^6 rays were required to predict sound-pressure levels that were similar within 1 dB for symmetric receiver locations with a cell side-length of 10 cm. 10^7 rays were required for similar accuracy if a receiver side-length of 5 cm was used. Sound-pressure levels were then predicted between a source and a single reflecting surface of infinite impedance. It was found that

a receiver resolution of 5 cm was sufficient to represent the modal behaviour of the sound field. Prediction using 1 Million rays produced results within 2 dB of theory. Since someone with good hearing can only distinguish differences of 1 dB, receiver cells of 5 cm and 1 Million rays were used in the prediction throughout this research.

The sound-pressure level between a source and a wall of complex reflection coefficient was also validated. The resulting prediction placed nodes in the sound-pressure level in appropriate locations as defined by the input complex reflection coefficients.

The steady-state intensity algorithm was validated in anechoic and diffuse environments. Results for an anechoic room with one or two sources were highly accurate. The direction of the predicted intensity vector in the diffuse room was accurate as well.

The transient-intensity modification was validated by predicting the time-dependent intensity directions over a surface for various diffusion coefficients. The resulting "I-echogram" distinguished a greater number of ray-receiver paths for larger diffusion coefficients.

The validated program was compared with experimental sound-pressure levels and sound-intensity levels. To achieve this, the complex reflection coefficients of plywood, carpet, drywall, and acoustical ceiling tile were measured using an impedance-tube method and the spherical-decoupling method. Prediction of sound-pressure levels between a source (normal and oblique incidence) and the four characterized surfaces were much more accurate that the original predicted levels. Using the reflection coefficients found by the spherical-decoupling method, sound-pressure levels at frequencies lower than 1000 Hz were usually within 2 dB of those measured. Prediction accuracy at 1000 Hz was not as good, although locations of nodes and anti-nodes were usually correctly predicted. The complex reflection coefficients calculated using a previously implemented impedance tube method were incorrect, prediction using these values as parameters were rarely accurate.

The steady-state 3D intensity levels were compared with those found in the anechoic chamber over the characterized surfaces for various receiver heights. Resulting

intensity directions were most accurate at higher frequencies where the complex reflection coefficients of the reflecting surfaces were less irregular, and therefore known with more confidence, than those at lower frequencies. Steady-state intensity accuracy was also greatest at receiver positions that were neither close to the source nor the reflecting surface, where the plane-wave assumption is valid, and where near-field and edge-diffraction effects are limited. Accuracy could be improved if the surfaces were characterized at the exact receiver height used in the comparison.

Sound-pressure levels predicted and measured in a scale-model room were accurate within 5 dB, with most node and anti-node levels within 2 dB. Results at 1000 Hz agreed less well; a finer measurement resolution is required to investigate the reasons for this. This scale-model room used was poorly sealed at its edges; for this and other reasons a full-scale room was used for further comparison.

In a full-scale room, the sound-pressure level prediction accuracy was frequency-dependent. Agreement was less than that of RAYCUB, but similar modal responses were predicted. At higher frequency (1000 Hz), the new model was less accurate than the original version since it predicted a modal behaviour that was completely absent in the measured sound field. It was demonstrated that the diffusion coefficient of boundaries affect the predicted sound field to a great extent. It was explained that ORAYCUB, unlike RAYCUB, could be used to inversely determine the boundary conditions, such as the diffusion coefficient, by finding the parameters that best fit measured sound-pressure levels. 3D intensity comparison in the same room agreed relatively well, with two thirds of the cases accurate within 25^{o}; a significant portion of the predicted intensity directions were accurate within 15^{o}. Further comparison of predicted pressure and intensity levels in a full-scale room, with regular un-interrupted surfaces having well-known complex refection coefficients, is needed before a definitive evaluation of the new program's effectiveness in real rooms can be made.

A final discussion on the sources of error is this work was given. Important sources of error include measurement-location uncertainty and the use of directional loudspeaker sources. All sources were modeled as omni-directional point sources.

Chapter 8

The objectives of this work have been accomplished, proven by validation, and measurement comparison with sound-pressure levels and sound-intensity levels measured in the presence of one reflecting surface, in an otherwise anechoic chamber.

Future Work

Despite the numerous improvements to the original ray-tracing model outlined in this work which increased the accuracy of prediction in the anechoic chamber, and near a reflecting surface, there are many opportunities for future improvements to the model. Presently, the model uses a cubic receiver volume which causes poor prediction accuracy near a source because the spherical wave front of the sound waves is approximated using squares with side length equal to the receiver cell side length. This results in a faceted spherical surface that is increasingly inaccurate the closer the wave front is to the source. Using a spherical receiver alleviates this problem, and is an important modification that should be made. In the current model, the intensity level prediction is limited to being predicted for a single receiver location. This could be modified to allow ORAYCUB to predict the intensity levels over all receiver positions on a horizontal plane, as is the case for predicting sound-pressure level.

Further comparison with full-scale rooms is also suggested, since strong conclusions on the program's accuracy in these rooms were not made due to having insufficient data. With the model's present accuracy near a reflecting surface, ORAYCUB provides the user with a tool that could be used to investigate the effect of the diffusion coefficient, compare it with theory, and compare prediction of SPLs with measured data using surfaces with varying diffusion coefficients.

Bibliography

[1] L. De Geetere. Analysis and improvement of the experimental techniques to assess the acoustical reflection properties of boundary surfaces. PhD dissertation, Katholieke Universiteit Leuven, 2004.

[2] H. Kutruff. *Room Acoustics*. Applied Science Publishers Ltd, London, England,1973.

[3] M.A. Hamdi and L. Mebarek. Capabilities and limitations of boundary and finite element methods for solving noise and vibration problems. *Journal of the Acoustical Society of America*, 102:5, 1997.

[4] J.B. Allen and D.A. Berkely. Image method for efficiently simulating small-room acoustics. *Journal of the Acoustical Society of America,* 65:4, 1979.

[5] A.M. Ondet and J.L. Barbry. *Modelisation de la Propagation dans les Locaux Industriels Encombres a Partir de la Technique des Rayons – Logiciel Rayscat.* N.S.T. nº 67 INRS, 1987.

[6] A. Farina. Pyramid tracing vs. ray tracing for the simulation of sound propagation in large rooms. *Computational Acoustics,* Computational Mechanics Publications, 1995.

[7] J.S. Suh and P.A. Nelson. Measurement of transient response of rooms and comparison with geometrical acoustic models. *Journal of the Acoustical Society of America,* 105:4, 1999.

[8] A. Wareing. Acoustical modeling of rooms with extended-reaction surfaces. M.A.Sc. Thesis, The University of British Columbia 2000.

[9] G. Wong. Measurement and prediction of low frequency noise in industrial Workshops. M.A.Sc. Thesis, The University of British Columbia, 2005.

[10] M. Hodgson. Evidence of diffuse surface reflections in rooms. *Journal of the Acoustical Society of America,* 89:2, 1991.

[11] G. Chan. Prediction of Low-Frequency Sound-Pressure Fields in Fitted Rooms for Active Noise Control. M.A.Sc. Thesis, The University of British Columbia, 2008.

[12] L. Cremer and H. Muller. *Principles and Applications of Room Acoustics Vol 1.* Applied Science Publishers Ltd, London, England, 1982.

Bibliography

[13] ASTM-E1050-98, *Impedance and Absorption of Acoustical Materials Using a Tube, Two Microphones and Digital Frequency Analysis System*. ASTM International, 1998.

[14] Y. Champoux and J.F. Allard. Measurement of acoustic impedance of sound absorbing materials in a free field at low frequencies. *Journal of the Acoustical Society of America,* 82:S1, 1987.

[15] F.J. Fahy. *Sound Intensity*. Elsevier Applied Science, London, England, 1989.

[16] L.E. Kinsler and A.R. Frey. *Fundamentals of Acoustics.* John Wiley & Sons, Inc, New York, United States of America, 1950.

[17] Y.W. Lam. A comparison of three diffuse reflection modeling methods used in room acoustics computer models. *Journal of the Acoustical Society of America,* 100:4, 1996.

[18] J.F. Li and M. Hodgson. Use of pseudo-random sequences and a single microphone to measure surface impedance at oblique incidence. *Journal of the Acoustical Society of America,* 102:4, 1997.